Article

Not peer-reviewed version

Novel Copper(II) Coordination Compounds Containing Pyridine Derivatives of N^4-methoxyphenyl-Thiosemicarbazones with Selective Anticancer Activity

Roman Rusnac , Olga Garbuz * , Victor Kravtsov , Elena Melnic , Dorin Istrati , Victor Tsapkov , Donald Poirier , Aurelian Gulea *

Posted Date: 26 November 2024

doi: 10.20944/preprints202411.1900.v1

Keywords: coordination compounds; $N^{(4)}$-methoxy-phenyl thiosemicarbazones; anticancer agents; molecular structure; antioxidant activity; toxicity; selectivity

Article

Novel Copper(II) Coordination Compounds Containing Pyridine Derivatives of N⁴-methoxyphenyl-Thiosemicarbazones with Selective Anticancer Activity

Roman Rusnac [1], Olga Garbuz[2,*], Victor Kravtsov[3], Elena Melnic[3], Dorin Istrati[4], Victor Tsapkov[1], Donald Poirier[5] and Aurelian Gulea[1,*]

[1] Laboratory of Advanced Materials in Biopharmaceutics and Technics, Institute of Chemistry, Moldova State University, 60 Mateevici Street, MD-2009 Chisinau, Moldova; roman.rusnac@usm.md (R.R.); victor.tapcov@usm.md (V.T.); guleaaurelian@gmail.com, guleaaurelian@gmail.com (A. G.)
[2] Laboratory of Systematics and Molecular Phylogenetics, Institute of Zoology, Moldova State University, 1 Academiei Street, MD-2028 Chisinau, Moldova; olhamos1@gmail.com (O. G.)
[3] Laboratory of Physical Methods of Solid State Investigation "Tadeusz Malinowski", Institute of Applied Physics, Moldova State University, 5 Academiei Street, MD-2028 Chisinau, Moldova; victor.kravtsov@ifa.md (V.K.); elena.melnic@ifa.usm.md (E.M.)
[4] Department of Dentistry, University of Medicine and Pharmacy "Nicolae Testemitanu", 165 Stefan cel Mare si Sfant Bd., MD-2004 Chisinau, Moldova; dorin.istrati@usmf.md (D. I.)
[5] Laboratory of Molecular Endocrinology at Laval University Medical Research Center, Quebec, Canada; donald.poirier@crchudequebec.ulaval.ca (D.P.)
* Correspondence: olhamos1@gmail.com, olga.garbuz@sti.usm.md (O. G.), aurelian.gulea@usm.md, guleaaurelian@gmail.com (A. G.)

Abstract: Ten coordination compounds: [Cu(L¹)Cl] (C1), [Cu(L¹)NO₃] (C2), [Cu(L²)Cl] (C3), [Cu(L²)NO₃] (C4), [Cu(L³)Cl] (C5), [Cu(L³)NO₃] (C6), [Cu(L⁴)NO₃] (C7), [Cu(L⁴)Cl] (C8), [Cu(L⁵)Cl] (C9), [Cu(L⁵)NO₃] (C10) containing pyridine derivatives of *N*⁴-methoxyphenyl-thiosemicarbazones were synthesized and characterized. The molecular structure of four compounds was investigated using single crystal X-ray diffraction. Spectral analysis techniques such as FT-IR, ¹H, ¹³C-NMR, and elemental analysis and molar conductivity were used for all the synthesized compounds. The tested synthesized compounds were evaluated for their anticancer activity and selectivity against a variety of cancer cell lines, including LNCaP, MCF-7, HepG-2, K-562, HeLa, BxPC-3, and RD and normal cell line. Most compounds demonstrated selective anticancer activity superior to doxorubicin. Notably, all ligands showed high antiproliferative activity against HL-60 cells, with IC_{50} values between 0.01 and 0.06 μM, and a selectivity index as high as 10000. Coordination of copper with proligands HL^1 and HL^3 notably enhanced antiproliferative activity, lowering the IC_{50} to 0.03 μM. Additionally, the antioxidant activity of these compounds was assessed, revealing that all tested ligands and most coordination compounds exhibited greater antioxidant activity compared to Trolox, with some ligands showing activity up to 12.3 times higher. Toxicity studies on *Daphnia magna* indicated low toxicity for the ligands, generally less than doxorubicin, with LC_{50} values ranging from 13 to 90 μM, suggesting moderate toxicity. Conversely, the coordination complexes were more toxic, with LC_{50} values between 0.5 and 13 μM.

Keywords: coordination compounds; *N*⁽⁴⁾-methoxy-phenyl thiosemicarbazones; anticancer agents; molecular structure; antioxidant activity; toxicity; selectivity.

1. Introduction

Heterocyclic compounds with a pyridine ring play an important role in the biochemical processes of living organisms; a majority of medical products contain heterocyclic fragments, especially azabenzene rings. Natural products such as nicotinic acid, nicotine, anabasine, pyridoxine, and castor oil contain pyridinic rings, as do synthetic products such as isoniazid, pioglitazone,

 doi:10.20944/preprints202411.1900.v1

lansoprazole, and sulphapyridines [1]. The class of organic compounds called thiosemicarbazones in the last decade has been studied. Hundreds of articles are reported in the specialized literature with different techniques for their synthesis: a) condensation between aldehyde or ketone and thiosemicarbazide [2]; b) nucleophilic addition between insothiocyanate and hydrazone [3]; c) from carbon disulfide [4,5] and reactions with hydrazine monohydrate followed by transamination reaction with a higher amine [6]. Adding pyridin-2-yl fragments to the thiosemicarbazone skeleton makes it much more effective an anticancer activity [7–9]. Since the discovery of anticancer molecules based on thiosemicarbazone fragments, some potential drugs have been evaluated [10–13]. However, the majority of these thiosemicarbazones give insufficient selectivity [14].

The methoxy group can be found in many drugs, such as trimethoprim, phenacetin, etc., that can participate in the transmethylation mechanism [15,16]. Heterocyclic thiosemicarbazones exhibit a wide spectrum of biological activities, such as antibacterial [17–24], antiviral [25–27], antiparasitic [28], antifungal [29,30] antimalarial [31,32], and particularly anticancer activity [28,33–37] but also in a catalytic perspective [38].

The aim of this study is to synthesize and characterize compounds, and to evaluate their anticancer activity and selectivity against various cancer cell lines, including LNCaP, MCF-7, HepG-2, K-562, HeLa, BxPC-3, and RD. A key aspect of this research is the incorporation of the methoxy-phenyl fragment (Figure 1) into the thiosemicarbazone skeleton, which is expected to enhance membrane permeability in cancer cells and decrease the toxicity of the synthesized compounds by increasing their molecular lipophilicity.

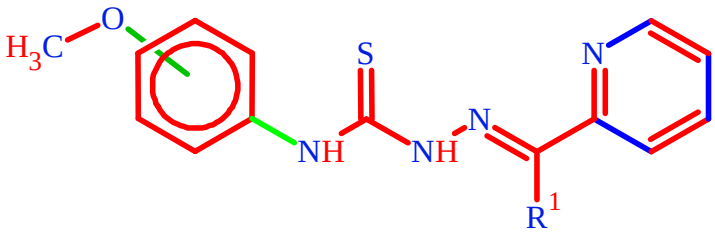

Figure 1. The general formula of the thiosemicarbazones **HL**$^{1\text{-}5}$.

2. Results and Discussion

We directed our research to the synthesis of thiosemicarbazones that have the methoxyphenyl moiety substituted in the 4-position of thiosemicarbazide. We carried out the synthesis of ligands **HL**$^{1\text{-}5}$ using two routes; method A involves the classic reaction between 2-pyridinecarboxaldehyde (Scheme 1) and the corresponding thiosemicarbazide, as described in [39–41].

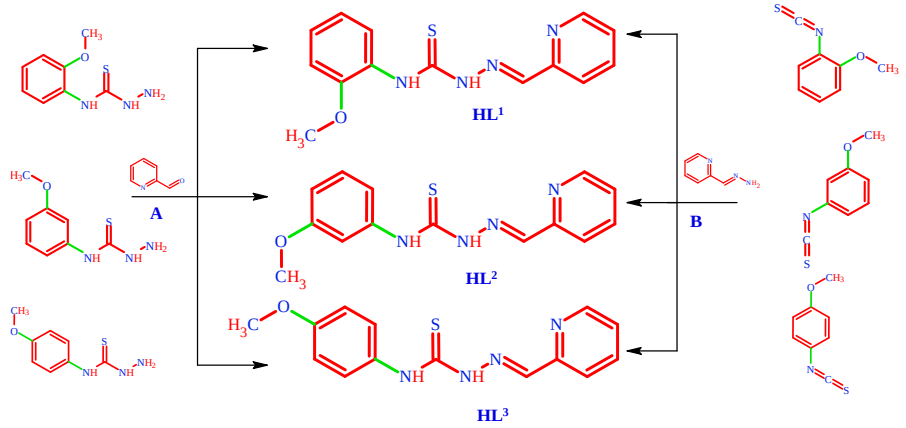

Scheme 1. Synthesis of **HL**$^{1\text{-}3}$ N-({2/or 3 /or 4}-methoxyphenyl)-2-[(pyridin-2-yl)methylidene]-hydrazine-1-carbothioamide.

 doi:10.20944/preprints202411.1900.v1

Method B for the synthesis of thiosemicarbazones **HL**[1-5] by the nucleophilic addition reaction between 1-isothiocyanato-2-methoxybenzene or its derivatives with hydrazones (Schemes 1 and 2). Leads to the formation of synthesis products with high purity and quantitative yield.

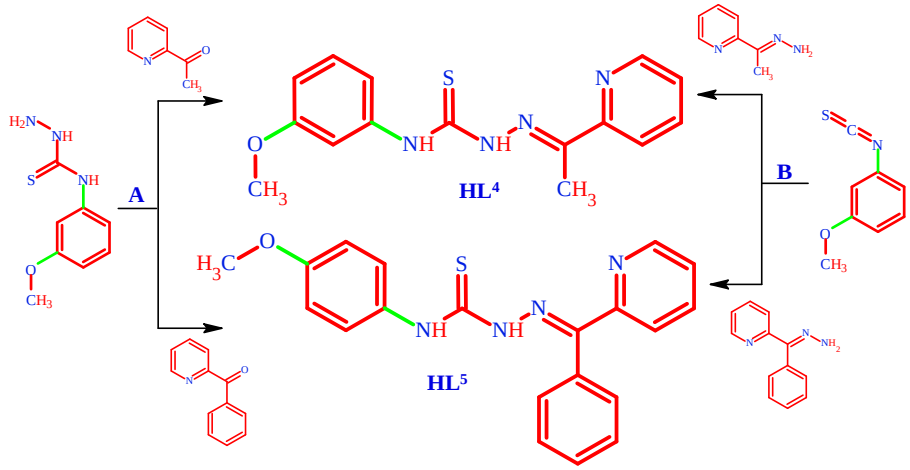

Scheme 2. Synthesis of **HL**[4], **HL**[5] N-(3-methoxyphenyl)-2-[1-(pyridin-2-yl)ethylidene]hydrazine-1-carbothioamide and N-(4-methoxyphenyl)-2-[phenyl(pyridin-2-yl)methylidene]hydrazine-1-carbothioamide.

The thiosemicarbazones **HL**[1-5] were characterized by FTIR; the azomethine group >C=N[30], can be found in the IR spectrum at 1585-1570 cm^{-1}, which corresponds to uncoordinated azomethine groups . The presence in the IR spectra of free ionic group ligands (C=S) at 1260-1245 and 830-845 [42] cm^{-1} corresponds to the uncoordinated ligand, and upon coordination with 3*d* metal ions, they lead to a shift to lower wavenumbers such as 1230-1210 cm^{-1}. In the case of coordinative compounds **1-10**, we only find valence vibrations (C-S) at 730-785 cm^{-1}, which tell us about the formation of a metal-sulfur (ionic) bond at wave numbers 460-510 cm^{-1}[43].

According to [44], the ^{1}H-NMR analysis revealed the presence of a more N-H (hydrazinic) acidic proton at 14–12 ppm, which [9,39,45]. In the range of 3.70 to 3.80 ppm. The O-CH_3 group from the structure of thiosemicarbazones HL[1–5]. We find the presence of -N4H- at 8.00-8.35 ppm in the free uncoordinated ligands. We can see the C=S group[46,47] in HL[1-5] ligands at 176.1–177.8 ppm in the ^{13}C-NMR spectrum. Only one tautomeric tionic form is present in solution [48,49].

2.1. Structure description of HL[2], HL[3], HL[5] and complex C3a

Crystals of **HL**[2] belong to the monoclinic space group $P2_1/c$, their structure reveals that molecules are about planar with deviation of non-hydrogen atoms from their common plane within 0.07 Å the thiosemicarbazone fragment has E configuration, (Figure 2 a). The planarity of the molecule is supported by an intramolecular N1-H···N3=2.626(3) Å hydrogen bond. In the crystal structure the intermolecular N2-H···N4= 3.043(3) Å bonds unite the molecules in the herringbone like chains along the *b* crystallographic axis (Figure 2 b)

 doi:10.20944/preprints202411.1900.v1

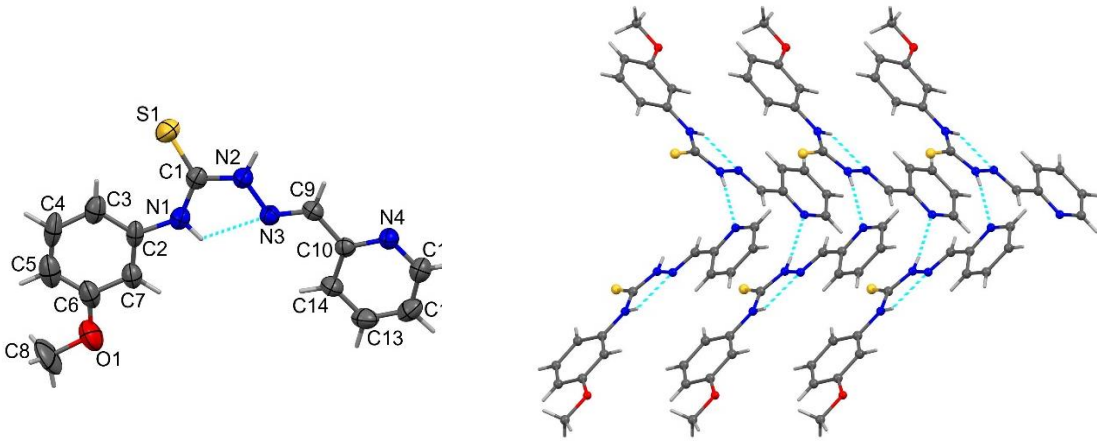

(a) **(b)**

Figure 2. The view of molecule **HL²** with numbering scheme **(a)**, the herringbone like chains running along *b* crystallographic axis in the crystals **(b).**

The crystals of **HL³**, were separated in the form of the dehydrate $HL^3 \cdot 2H_2O$, belong to the centrosymmetric triclinic space group *P*-1(Table 3) and the asymmetric unit contains two identical molecules (A and B) and two water molecules (Figure 3 a). The thiosemicarbazone fragment of the molecule **HL³** adopts an *E* configuration, similar to **HL²,** but molecule orientation of the pyridine substitution differs in **HL²** and **HL³** by the *trans*- and *cis*-position of the pyridine N4 atom with respect to the hydrazine N3 atom. The overlay of molecules A (magenta line) and B (green line) shows their similar conformations (Figure 3 b). The molecules are non-planar and the dihedral angles between the N^4-methoxyphenyl fragment and the rest of the molecule are 46.96° and 44.86° for molecules A and B, respectively, due to rotation around single N1-C2 bonds. The corresponding torsion angles C1-N1-C2-C3 are 49.08° and 45.62° for molecules A and B, respectively.

In the crystal, each of the independent molecules A and B forms a centrosymmetric supramolecular dimer through a pair of N2A···S1A 3.373(5) Å and N2B···S1B 3.436(5) Å hydrogen bonds, respectively. In each dimer, H-bonds form $R^2_2(8)$ graph sets. These dimers are linked through water dimer $2(H_2O)$ by intermolecular N-H···O hydrogen bonds, forming chains in which the dimer of molecules A and the dimer of molecules B alternate with water dimer (Figure 3 c, Table S2).

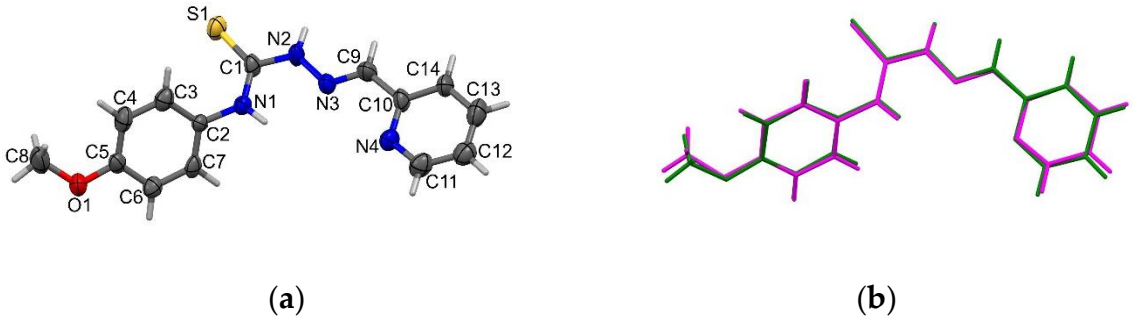

(**a**) (**b**)

Preprints.org (www.preprints.org) | NOT PEER-REVIEWED | Posted: 26 November 2024 doi:10.20944/preprints202411.1900.v1

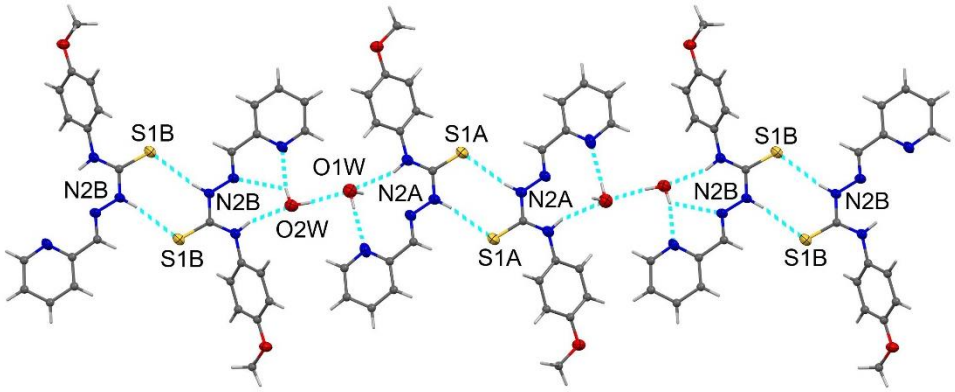

(**c**)

Figure 3. View of the **HL**[3] molecule with numbering scheme (a), molecular overlay in **HL**[3] (b), the supramolecular chain in **HL**[3] (**c**).

The **HL**[5] crystals crystallizes in the monoclinic space group $P2_1/n$ (Table 3). In this the structure, of **HL**[5] the thiosemicarbazone fragment also adopts an E configuration, but in contrast to to **HL**[2] and **HL**[3] this ligand differs in the position of the pyridine substituent with respect to the double azomethine bond N3-C9. In **HL**[2] and **HL**[3] the N2–N3═C9–C10 fragment has an E configuration while in **HL**[5] it has a Z configuration. The conformation of the molecule is supported by two intramolecular N-H···N hydrogen bonds, (Table S2) providing planarity of the molecule within (0.11 Å) except for the phenyl substituent at the C9 atom, which forms a dihedral angle of 44.56° with the rest of the molecule. The crystal structure reveals intermolecular π–π stacking interactions between center symmetry related pyridine and anisole fragments with a Cg-Cg distance of 3.924 Å, resulting in the formation of a supramolecular dimer (Figure 4 a).

Complex **C3a** crystallizes in the monoclinic space group $P2_1/c$ (Table 3). Structural studies revealed that **C3a** is a centrosymmetric neutral dimeric compound with the formula $[Cu_2(L^2)_2Cl_2]\cdot 2DMF$, in which Cl(1) atoms serve as bridging ligands (Figure 4 b). Upon complexation with Cu(II), the ligand L^2 undergoes a configurational change of the thiosemicarbazone moiety from the *E* to the *Z* form, favouring the tridentate chelating coordination form. The Cu1 atom in the formed dimer **C3a** is pentacoordinate and the copper center exhibits a distorted square-pyramidal coordination (τ =0.158). The tridentate thiosemicarbazone ligand is coordinated to the central atom in the monodeprotonated form (L^2) using an NNS set of donor atoms (Figure 4b), forming two fused five-membered CuSCNN and CuNCCN metallacycles, with the dihedral angle between their mean planes being 3.52°. The bond distances in the coordination polyhedron Cu(1)–N(3), Cu(1)–N(4), Cu(1)–S(1), Cu(1)–Cl(1) and Cu(1)–Cl(1)* equal 1.962(4), 2.045(3), 2.257(1), 2.236(1), and 2.925(1) Å, respectively (Table S1). Two DMF solvent molecules form N1-H···O1D= 2.922(6) Å hydrogen bonds with the dimeric complex.

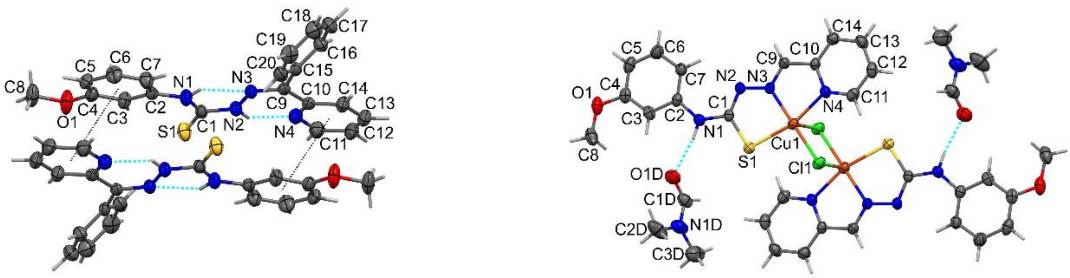

(**a**) (**b**)

Figure 4. Supramolecular dimmer in **HL**[5] stabilized by intermolecular π–π stacking interactions **(a);** molecular structure of the coordination compound **C3a (b).**

 doi:10.20944/preprints202411.1900.v1

2.2. Biological Activity

2.2.1. Anticancer activity and selectivity

Antiproliferative activity (APA) is defined by the ability of compounds to inhibit the growth and division of cells. Compounds exhibiting antiproliferative activity may induce cell cycle arrest, promote apoptosis, or alter cell signaling pathways involved in growth regulation.

Research indicates that substances with high antioxidant activity may also possess some anticancer properties. However, this is not always the case, the presence of antioxidant activity does not guarantee that a compound will exhibit significant antiproliferative activity. For instance, some compounds may effectively neutralize free radicals but have little to no direct impact on cells. Thus, comparing antioxidant and antiproliferative activities is essential for understanding the potential therapeutic effects of various compounds. A deeper exploration of the relationship between AOA and antiproliferative activity may lead to the development of more effective drugs that can simultaneously protect cells from oxidative stress and inhibit the growth of cancer cells.

High and low selectivity continue to pose significant challenges in cancer management, despite advancements in anticancer therapy. Chemotherapy often results in severe side effects due to its cytotoxic effects on normal cells, which limits its use and may require dose reduction, interruption, or even cessation of treatment. Therefore, it is crucial for anticancer drugs to demonstrate high selectivity, targeting tumor cells specifically while sparing normal cells. This emphasis on selectivity is essential, as agents with higher selectivity reduce toxicity to normal cells and enhance safety. Consequently, the primary goal in cancer chemoprevention remains the discovery of new agents that are both effective and possess high selectivity.

Antineoplastic agents are divided into cytotoxic and cytostatic. Doxorubicin, cisplatin, fluorouracil, hydroxyurea, cyclophosphamide are most known among the cytostatic drugs. Doxorubicin, a frontline drug regarded as one of the most potent of the Food and Drug Administration (FDA) approved chemotherapeutic agents, has been used in cancer treatment for more than 30 years. Doxorubicin causes toxicity to most major organs, especially cardiotoxicity while providing a cure in select cases, which forces the treatment to become dose-limiting. DOXO cardiomyopathy is known to have a poor prognosis and is frequently fatal. DOXO causes toxic damage to the mitochondria of cardiomyocytes contributing to enhanced oxidative stress [50,51].

Platinum-based anticancer drugs also play a leading role in the treatment of various malignant tumors, but severe side effects such as nephrotoxicity, neurotoxicity, and drug resistance have limited their wide range of clinical applications [52,53]. This has stimulated extensive research and has promoted chemists to establish alternative approaches on the basis of using endogenous metals to improve the pharmacological properties. Copper complexes are considered promising alternatives to platinum complexes as anticancer drugs because copper is biocompatible and plays many significant roles in biological systems. Also, copper shows the altered metabolism of cancer cells and differential response between normal and tumor cells. It is proven that the concentration of copper in cancerous tissues exceeds that of normal tissue, and the sequestration of copper can prevent the establishment of new blood vessels. Therefore, cancer cells may represent a suitable, selective target for copper-based agents[54, 55].

Different models like cancer cell lines, tumor explants, and enzyme systems are used to develop anticancer substances, but selection mainly relies on cancer cell lines. Assessing the antiproliferative activity of compounds serves as an initial screening approach for potential drug candidates.

In this study, we examined the antiproliferative activity of the synthesized compounds against various cell lines, including human cervical adenocarcinoma epithelial cell HeLa line, human pancreatic adenocarcinoma epithelial cell BxPC-3 line, human multinucleated rhabdomyosarcoma muscle cell RD line, human peripheral blood acute promyelocytic leukemia promyeloblast cell HL-60 line, human prostate carcinoma cell LNCaP line, human breast carcinoma cell MCF-7 line, human hepatocellular carcinoma cell HepG-2 line, human chronic myeloid leukemia bone marrow cell K-562 line, and normal canine kidney epithelial cell MDCK line. Therefore, our investigation provides

 doi:10.20944/preprints202411.1900.v1

valuable insights that can facilitate the preliminary screening of these substances for their anticancer activity, potentially leading to the identification of new therapeutic agents in oncology.

The antiproliferative activity of the tested compounds was compared with the anticancer agents doxorubicin and cisplatin. The data are presented in Tables 1 and 2. For a comparative assessment of the results, IC_{50} (μM) values were used as quantitative indicators of the efficacy of the antagonist substances in determining the optimal therapeutic dose.

The data in Table 1 indicate that doxorubicin and cisplatin exhibit high toxicity, with a low selectivity index ranging from 0.05 to 1.8. Both anticancer agents demonstrate significant anticancer activity against the studied cell lines, with doxorubicin showing greater activity compared to cisplatin. Furthermore, both substances possess antioxidant activity, with the activity of doxorubicin exceeding that of Trolox. A correlation is observed between the antioxidant activity and anticancer activity of doxorubicin (DOXO) and cisplatin (CDDP) toward the HeLa and BxPC-3 cancer cell lines.

The obtained results regarding the antiproliferative activity of the synthesized copper(II) metal coordination compounds with thiosemicarbazone ligands **HL, HL** $^{1\text{-}5}$ on HeLa, RD, BxPC-3 cancer cell lines, as well as MDCK normal cell line are shown in Table 1.

To demonstrate the selectivity of the antiproliferative activity for these cancer cell lines, the IC_{50} values for the MDCK normal cell line were used to calculate the selectivity indexes (SI). The SI was determined by taking the ratio of the IC_{50} value for the normal cell line to the IC_{50} value for the cancer cell line, as per Formula:

$$\boldsymbol{SI = \frac{IC_{50}\ (MDCK)}{IC_{50}\ (\text{cancer cell line})}}$$

Table 1. Antiproliferative activity and selectivity of the tested compounds against HeLa, RD, and BxPC-3 cancer cell lines, as well as MDCK normal cell line.

	MDCK	BxPc-3		RD		HeLa	
Compound	**IC_{50}, μM**	**IC_{50}, μM**	**SI**	**IC_{50}, μM**	**SI**	**IC_{50}, μM**	**SI**
DOXO	10.8	6	1.8	16.2	0.7	6.2	1.7
CDDP	1.5	11.2	0.1	4.6	0.3	30.9	0.04
HL	100	100	1	1.1	90.9	8.3	12.0
HL^1	10.1	0.1	101	100	0.1	81.2	0.1
HL^2	0.4	0.1	4	0.2	2.0	0.1	4.0
HL^3	100	2.1	48	0.5	200	100	1.0
HL^4	14.9	0.1	149	11.6	1.3	5.8	2.6
HL^5	100	3.2	31	0.5	200	100	1.0
$[Cu(L^1)Cl]$ **(C1)**	0.3	0.1	3	0.1	3.0	0.8	0.4
$[Cu(L^1)NO_3]$ **(C2)**	0.6	0.1	6	0.1	6.0	0.8	0.8
$[Cu(L^2)NO_3]$ **(C4)**	1.3	0.1	13	0.1	13	0.1	13.0
$[Cu(L^3)Cl]$ **(C5)**	26.6	9.4	3	19.7	1.4	26.1	1.0
$[Cu(L^3)NO_3]$ **(C6)**	2.1	0.11	19	1.2	1.8	1.1	1.9
$[Cu(L^4)NO_3]$ **(C7)**	0.9	0.2	5	0.5	1.8	0.1	9.0
$[Cu(L^4)Cl]$ **(C8)**	1.1	0.1	11	0.2	5.5	0.1	11.0
$[Cu(L^5)Cl]$ **(C9)**	13.1	0.1	131	0.2	65.5	3.9	3.4

 doi:10.20944/preprints202411.1900.v1

[Cu(L^5)NO$_3$] **(C10)**	0.2	0.2	1	0.3	0.7	0.07	2.9

Average results of three experiments, SEM < ±3%.

First of all, the majority of the tested compounds demonstrated higher antiproliferative activity and selectivity compared to doxorubicin and cisplatin. The analysis of the data from this table shows that, in general, the tested compounds exhibited greater selectivity toward BxPC-3 and RD cells, for instance, the ligands **HL^1** and **HL$^{3\text{-}5}$** have selectivity indices (SI) ranging from 31 to 200, whereas doxorubicin (DOXO) and cisplatin (CDDP) have SI values from 0.1 to 2. Regarding HeLa cells, complexes **C5**, and **C6-9** possess higher SI values than DOXO and CDDP.

The thiosemicarbazones ligands **HL, HL $^{1\text{-}5}$**, as shown in Figure 5, demonstrated selective antiproliferative activity against tested cancer cell lines. The ligand *N*-phenyl-2-(pyridin-2-ylmethylidene)hydrazinecarbothioamide exhibited APA against HeLa, RD, and BxPC-3 cell lines within the following concentration IC$_{50}$ range: 1-100 μM. The presence of the phenyl group may enhance hydrophobic interactions, which could contribute to its overall activity. *N*-(2-methoxyphenyl)-2-(pyridin-2-ylmethylidene)hydrazinecarbothioamide has an IC$_{50}$ range of 0.1-100 μM. The methoxy group in the ortho position likely increases electron density on the aromatic system, enhancing its ability to to improved antiproliferative effects. *N*-(3-Methoxyphenyl)-2-(pyridin-2-ylmethylidene)hydrazinecarbothioamide displays an IC$_{50}$ range of 0.1-0.2 μM, indicating potent activity. The methoxy group at the meta position may allow for effective stabilization of the reaction intermediates and enhance the stability of the interactions ligand with cellular targets, resulting in increased potency against cancer cells. *N*-(4-methoxyphenyl)-2-(pyridin-2-ylmethylidene)hydrazinecarbothioamide presents an IC$_{50}$ of 0.5-100 μM. The para-positioned methoxy group can also enhance electron density and may contribute to favorable sterics and electronic interactions with protein targets in the cancer cells. However, its broader range of activity suggests it might require higher concentrations for effectiveness compared to the ligands with the methoxy group in the meta and ortho positions. *N*-(3-Methoxyphenyl)-2-[1-(pyridin-2-yl)ethylidene]-hydrazinecarbothioamide has an IC$_{50}$ of 0.1-11 μM, indicating very strong activity. The presence of the ethylidene substituent increases steric hindrance, potentially facilitating better binding to specific cellular targets and improving selectivity against cancer cells. The combination of the methoxy group and this structural modification enhances its overall efficacy. *N*-(3-Methoxyphenyl)-2-[phenyl(pyridin-2-yl)methylidene]-hydrazinecarbothioamide demonstrates an IC$_{50}$ of 0.5-100 μM. The presence of both the methoxy group and the phenyl substituent may create a favorable electronic environment and steric arrangement that enhances binding to biological targets.

The observed differences in the antiproliferative activity of these ligands can be attributed to the influence of their functional groups and the positioning of these groups within the molecules. The variation in chemical structures, particularly the presence, type, and spatial arrangement of methoxy and phenyl groups, significantly impacts their ability to interact with cancer cells. These structural features can affect solubility, permeability, and activity. Each ligand may interact with different cellular targets or pathways, leading to varying degrees of effectiveness against distinct cancer cell lines.

Coordination of the obtained pro-ligands to the 3*d* metal atoms leads to an enhancement of antiproliferative activity on HeLa, RD, BxPC-3 cancer cell lines [56]. In many cases, the complexes even surpass doxorubicin (DOXO) and cisplatin (CDDP) in terms of activity against these three cancer cell lines. The copper complexes C1-4 exhibited activity within the range of IC$_{50}$ values from 0.1 to 0.8 μM, while complexes **C6-C10** showed activity ranging from 0.07 to 3.9 μM. Notably, **[Cu(L^5)NO$_3$] (C10)** demonstrated the highest antiproliferative activity towards HeLa cells, with an IC$_{50}$ of 70 nM.

The observed enhancement in antiproliferative activity upon coordination with 3*d* metal atoms, such as copper, can be attributed to several factors. First, the coordination of the metal ions can facilitate the stabilization of the ligand structure, making the complexes more chemically reactive and biologically active. This reactivity is essential for the interaction of these compounds with cellular components, which can lead to increased potency against cancer cells.

 doi:10.20944/preprints202411.1900.v1

Second, while free ligands may exhibit certain degrees of activity, the presence of a metal center often allows for broader and more effective interactions with specific biological targets, such as DNA, proteins, or enzymes involved in cell proliferation and apoptosis. The metal ions can participate in electron transfer processes or catalytic reactions, enhancing the overall mechanism of action of the anticancer agents. Furthermore, the structural configuration and electron density around the complexes can significantly influence their ability to penetrate cell membranes and reach intracellular targets.

The obtained results for another 5 cancer cell lines, namely HL-60, LNCaP, MCF-7, HepG-2 and K-562, are presented in table 2. As in the previous case, in order to show the selectivity of the antiproliferative activity towards these types of cancer cells, the IC_{50} towards MDCK normal cell line are given alongside with IC_{50} values towards cancer cell lines, and the corresponding selectivity indexes are given.

Table 2. Antiproliferative activity and selectivity of the tested compounds against HL-60, LNCaP, MCF-7, HepG-2 and K-562 cancer cell lines.

Compound	HL-60		LNCaP		MCF-7		HepG-2		K-562	
	IC_{50}, μM	**SI**	**IC_{50}, μM**	**SI**	**IC_{50}, μM**	**SI**	**IC_{50}, μM**	**SI**	**IC_{50}, μM**	**SI**
DOXO	**1**	11	1,1	0,1	14,0	0,8	2,8	3,9	0,4	27
HL	0,04	2500	43,9	0,4	100	1,0	100	1,0	100	1,0
HL^1	0,04	253	100	9,9	10	1,0	0,8	12,6	10	1,0
HL^2	0,01	40	0,9	2,3	3,5	0,1	0,6	0,7	0,9	0,4
HL^3	0,01	10000	100	1,0	100	1,0	52	1,9	10	10
HL^4	0,06	248	100	6,7	55	0,3	3,1	4,8	16	0,9
HL^5	0,02	5000	8,07	0,1	5,2	19,2	0,3	333,3	0,1	1000
$[Cu(L^1)Cl]$ **(C1)**	35	0,01	45	150	100	0,003	68	0,04	64	0,005
$[Cu(L^1)NO_3]$ **(C2)**	0,03	20	0,8	1,3	0,1	6,0	0,4	1,5	0,5	1,2
$[Cu(L^3)NO_3]$ **(C6)**	0,03	70	0,3	0,1	0,6	3,5	0,6	3,5	0,03	70
$[Cu(L^5)Cl]$ **(C9)**	0,2	66	10	0,8	9,4	1,4	14	0,9	19	0,7
$[Cu(L^5)NO_3]$ **(C10)**	10	0,02	1	5,0	0,1	2,0	16	0,01	10	0,02

Average results of three experiments, SEM < ±3%.

All investigated ligands demonstrated high antiproliferative activity against HL-60 cells, with IC_{50} values ranging from 0.01 to 0.06 μM and a high selectivity index reaching up to 10000. Coordination of copper with the proligands **$HL^{1,3}$** significantly enhanced antiproliferative activity, reducing the IC_{50} value to 0.03 μM. In most cases, with regard to LNCaP, MCF-7, HepG-2, and K-562 cancer cell lines, the ligands exhibit selective activity, and it is often observed that copper enhances the antiproliferative activity of these cell lines.

 doi:10.20944/preprints202411.1900.v1

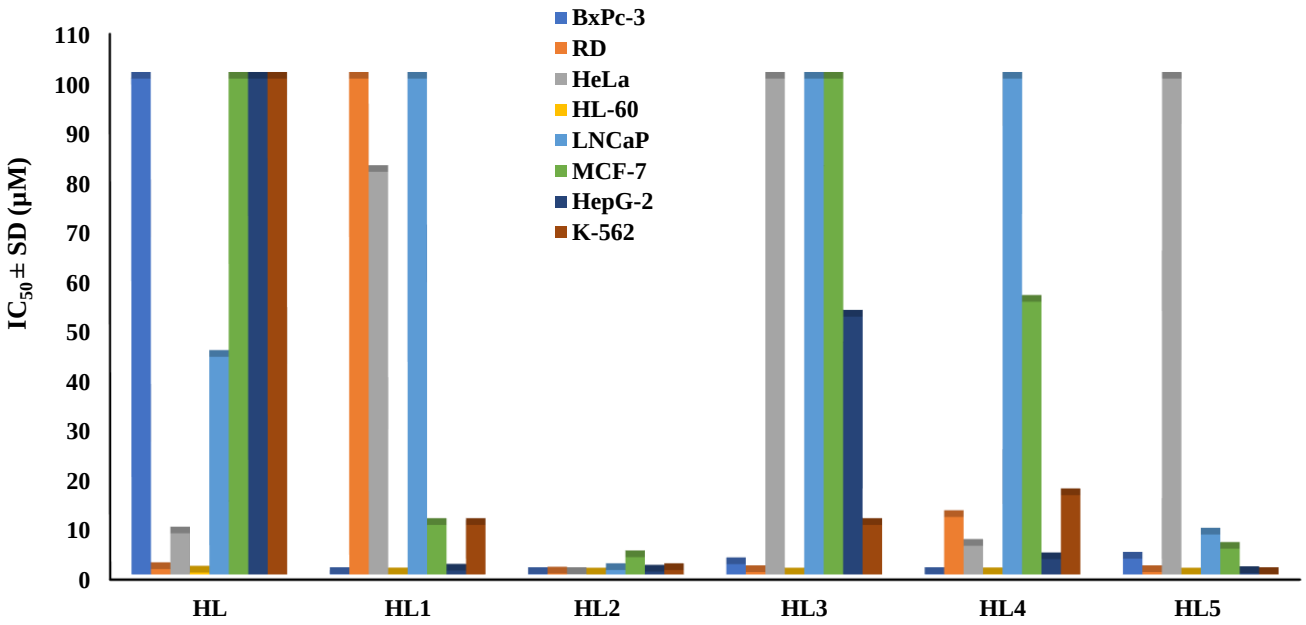

Figure 5. Inhibition of proliferation of HeLa, RD, BxPC-3, HL-60, LNCaP, MCF-7, HepG-2 and K-562 cancer cell lines by **HL, HL** [1-5]. Average results of three experiments, SEM < ±3%.

In summary, the antiproliferative activity of the tested ligands varies significantly, with the influence of functional groups and their positions playing a crucial role in determining their effectiveness. This diversity underscores their potential for personalized therapy.

In addition, the varying IC_{50} values among the copper complexes indicate the effect of different ligands and their coordination with copper on the antiproliferative potency. Overall, the results of this study highlight the importance of metal coordination in enhancing the biological activity of ligands and suggest a promising avenue for the development of new therapeutic agents in oncology.

2.2.2. Antioxidant Activity

Antioxidant activity refers to the ability of compounds to neutralize free radicals and prevent oxidative damage to cells. Antioxidants can donate electrons or hydrogen atoms to free radicals, making them less reactive. This protection enables cells to defend against damage caused by oxidative stress, which is a contributor to the pathogenesis of many diseases, including cancer. Antioxidant activity is often measured using method such as the $ABTS^{\bullet+}$. In our studies, the antioxidant activity of the tested compounds was measured using the $ABTS^{\bullet+}$ assay, with Trolox used as the standard for biochemical studies of antioxidant activity, alongside the anticancer drugs doxorubicin (DOXO) and cisplatin (CDDP) (Figure 6).

 doi:10.20944/preprints202411.1900.v1

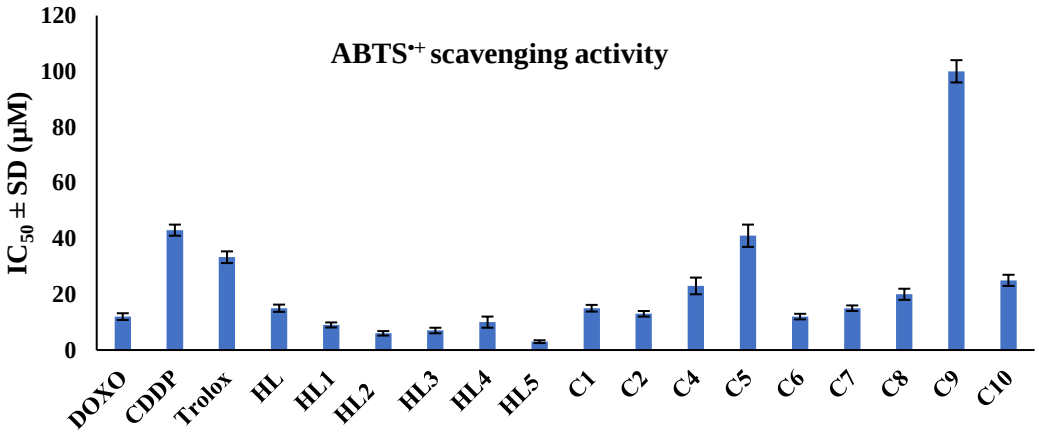

Figure 6. ABTS•+ scavenging activity of the ligants **HL, HL**[1-5], their coordination compounds, and DOXO, CDDP. .

According to the presented results, the thiosemicarbazones ligands **HL**[1-5] exhibit higher antioxidant activity than the copper(II) complexes of these thiosemicarbazones **HL**[1-5]. Additionally, all ligands demonstrated higher activity in comparison with Trolox, by up to 12.3 times.

The lowest antioxidant activity (IC_{50} = 14.9 μM) is observed for *N*-phenyl-2-(pyridin-2-ylmethylidene)hydrazinecarbothioamide (**HL**), which may be related to its structure lacking an additional methoxy group, potentially limiting its interaction with free radicals.

N-(2-methoxyphenyl)-2-(pyridin-2-ylmethylidene) (**HL**[1]**)** shows a significantly higher activity (IC^{50} = 9 μM), suggesting that the methoxy group positively influences receptor binding or reaction with free radicals. The next two ligands, *N*-(3-methoxyphenyl)-2-(pyridin-2-ylmethylidene)hydrazinecarbothioamide **HL**[2] and *N*-(4-methoxyphenyl)-2-(pyridin-2-ylmethylidene)hydrazinecarbothioamide **HL**[3], with IC_{50} values of 6.2 μM and 6.7 μM, respectively, exhibit similar activity levels. This indicates that the placement of the methoxy groups at the 3 and 4 positions of the thiosemicarbazides results in similar electronic distribution and stability. This suggests that while the positioning of functional groups on the phenolic ring is important for achieving high activity.

N-(3-Methoxyphenyl)-2-[phenyl(pyridin-2-yl)methylidene]hydrazinecarbothioamide (**HL**[5]), with an IC_{50} of 2.7 μM, demonstrates the highest antioxidant activity among the tested ligands. The methoxy group at position 3 and the phenyl group in another part of the structure may create a synergistic effect, enhancing activity through improved binding or a more effective electron transfer mechanism.

The coordination compounds of ligands HL and HL^{1-5} exhibited antioxidant activity in the following sequence: $[Cu(L^3)NO_3]$ (C6) ≥ $[Cu(L^1)NO_3]$ (C2) ≥ $[Cu(L^4)NO_3]$ (C7) ≥ $[Cu(L^1)Cl]$ (C1) ≥ $[Cu(L^4)Cl]$ (C8) ≥ $[Cu(L^2)NO_3]$ (C4) ≥ $[Cu(L^5)NO_3]$ (C10) ≥ $[Cu(L^3)Cl]$ (C5) ≥ $[Cu(L^5)Cl]$ (C9). The antioxidant activity of these coordination compounds can vary significantly due to their structural characteristics, electronic properties, types of ligands or anions, and the spatial arrangement within the molecule.

2.2.3. In vivo toxicity

In vivo toxicity studies are a crucial and mandatory phase in drug development, as they allow for the assessment of safety and potential risks associated with the use of new compounds. One method for studying toxicity involves testing on model organisms such as *Daphnia magna*. This species is widely used as a model organism in ecotoxicology, providing relevant data on toxicity at the organismal level. These organisms are sensitive to a variety of chemicals, making them important tools for evaluating potential threats to both the environment and human health.

 doi:10.20944/preprints202411.1900.v1

Research on *Daphnia magna* enables rapid assessment of the acute toxicity of compounds due to their short life cycle and high reproduction rate, allowing researchers to obtain results in a relatively short period of time. Testing methodologies using *Daphnia magna* are standardized and accepted by many international regulations, ensuring the comparability of results and facilitating further studies on other levels of toxicity and safety.

By studying the toxicity of new compounds in *Daphnia magna*, researchers can predict their impact on ecosystems, which is particularly significant for assessing the effects of drugs that may enter the environment through wastewater. Therefore, using *Daphnia magna* to evaluate acute toxicity is a justified and important step in the process of developing safe and effective pharmaceuticals, contributing to the reduction of potential risks to human health and the environment.

In this context, the substances were tested for toxicity Figure 7. The intensity of the influence of compounds at the median lethal concentration (LC_{50}) on *Daphnia magna* was determined through microanalysis. As expected, microscopy observations of Daphnia magna in the control group (without the tested compounds) indicated no pathological changes in the organisms. However, after incubation with the tested compounds, *Daphnia magna* were observed at the bottom of the wells. Light microscopy revealed that many of the *Daphnia magna* were moving slowly, while others remained motionless. Additionally, deformations were noted in the limbs and trunks of the *Daphnia magna*, with their internal contents mixed with the growth media [57].

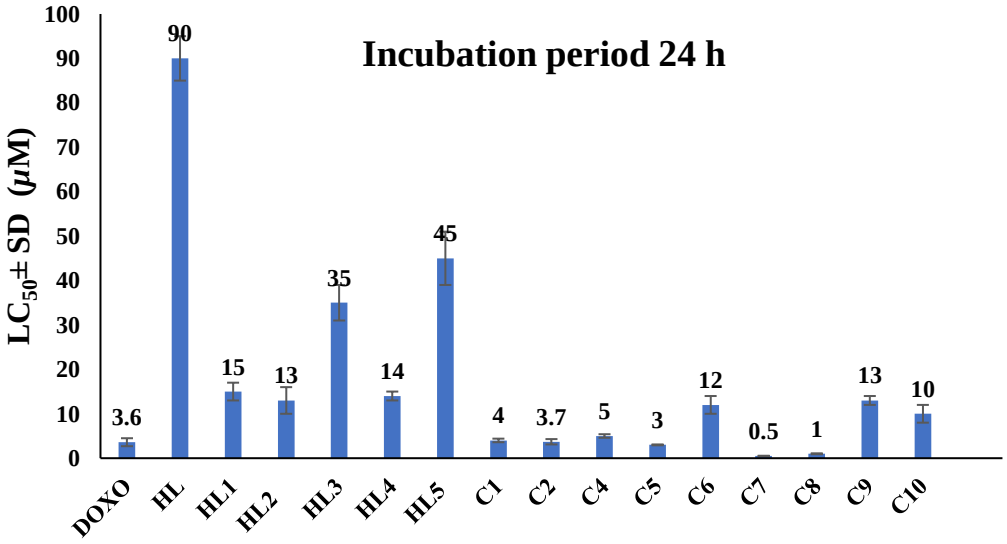

Figure 7. *In vivo* toxicity of the tested compounds and DOXO on *Daphnia magna* after 24 hours incubation.

Most of the tested substances exhibited lower or compared toxicity to doxorubicin. All ligands demonstrated less toxicity than the complexes formed with these proligands. The obtained LC_{50} values for the thiosemicarbazones **HL, HL** $^{1\text{-}5}$ range from 13 to 90 μM, indicating moderate toxicity. In contrast, the complexes showed higher toxicity, with LC_{50} values ranging from 0.5 to 13 μM. This indicates a significantly higher toxicity of the complexes compared to the proligands.

3. Materials and Methods

All the reagents used were chemically pure 3*d* metal salts $CuCl_2{\cdot}2H_2O$, $Cu(NO_3)_2{\cdot}3H_2O$ (Merck, Darmstadt, Germany) were used as supplied 2-Pyridinecarboxaldehyde; 2-Acetylpyridine; 2-Benzoylpyridine was used as received (Merck, Germany). Reagents and solvents were used as received from commercial sources.

3.1. Synthesis

 doi:10.20944/preprints202411.1900.v1

Tetramethylthiuram disulfide (1.5 equivalent) was added to a mixture of the respective anesidine derivatives (1.0 equivalent) and Dimethylformamide (10 mL). The reaction mixture was heated and stirred at 60-75 °C, 10-18 h The resulting mixture was concentrated by rotary evaporation. The precipitate formed upon cooling was collected by vacuum filtration and It was chemically purified by isolating the sulfur from the reaction medium after a 5% dissolution of thiourea in the mineral, then neutralized with sodium bicarbonate. The precipitate formed is recrystallised from toluene. Thioures are obtained as: *N*'-(2-methoxyphenyl)-*N,N*-dimethylthiourea (yield 79%); *N'*-(3-methoxyphenyl)-*N,N*-dimethylthiourea (yield 87%); *N*'-(4-methoxyphenyl)-*N,N*-dimethylthiourea (yield 95%).

The synthesis of thiosemicarbazides *N*-(2-methoxyphenyl)hydrazinecarbothioamide (yield 90%), *N*-(3-methoxyphenyl)hydrazinecarbothioamide (yield 94%); *N*-(4-methoxyphenyl)hydrazinecarbothioamide (yield 97%), occurs upon the interaction of thioureas with hydrazine monohydrate. The nucleophilic substitution reaction is carried out in p-xylene, at reflux temperature.

In the case of the chemical is observed degradation of thioureas with mineral acids in 1,4-dioxane, the formation of isothiocyanates occurs: 1-isothiocyanato-2-methoxybenzene (yield 76 %); 1-isothiocyanato-3-methoxybenzene (yield 67%), and 1-isothiocyanato-4-methoxybenzene (yield 94%).

The method A

General procedure

For the synthesis of thiosemicarbazone **HL** by method A: one equivalent of *N*-(x-methoxyphenyl)hydrazinecarbothioamide and one equivalent of the corresponding aldehyde or ketone are taken in a synthesis flask, dissolved in absolute ethanol, adding 10 mol% of glacial acetic acid to catalyze the end condensation reaction.

The method B

Synthesis of thiosemicarbazones **HL**$^{1\text{-}5}$ requires the reaction between the corresponding isothiocyanate and hydrazone (2-[hydrazinylidenemethyl]pyridine or 2-[1-hydrazinylideneethyl]pyridine or 2-[hydrazinylidene(phenyl)methyl]pyridines in a molar ratio of 1:1 dissolved in an aprotic solvent such as THF or 1,4-dioxane (note: it is recommended to avoid alcohols).

3.1.1.(. HL^{1}) N-(2-methoxyphenyl)-2-[(pyridin-2-yl)methylidene]hydrazine-1-carbothioamide

White crystalline solid, yield 98%; mp: 186-187°C, [58], R_f = 0.41 (ethyl acetate-toluene 2:1). Anal. Calc. for $C_{14}H_{14}N_4OS$: C(58.72%) H(4.93%) N(19.57%). Found: C(58.99%) H(5.04%) N(19.21%). FW: 286.35 g·mol^{-1}. ^{1}H NMR (400 MHz, DMSO-d_6) δ 14.47 (s, 1H, –N*H*-N), 12.10 (s, 1H, –N^4*H*), 10.04 (d, 1H, Py), 8.61 (d, 1H, Py), 8.60 (d, 1H, Py), 8.25 (d, 1H, Py), 8.01 (s, 1H, CH=N-), 7.91-6.96 (C-H, Ar), 3.87 (s, 3H, -O–CH_3). ^{13}C NMR (101 MHz, DMSO-d_6) δ 176.2 (C=S), 153.4 (HC=N), 152.7, 149.9, 143.1, 137.2, 128.0, 126.8, 125.7, 124.8, 120.5, 120.3, 111.9 (C-Ar and Py); 56.5(-O–CH_3). *The NMR spectra (**HL**$^{1\text{-}5}$) in detail in the Supplementary materials S1-10.* FTIR (cm^{-1}): 3279, 3143 ν (N-H, hydrazinic and thioamide); 3076 ν (C-H, aryl); 2960 ν_{as}(C-H) -CH_3); 2834 ν_{sy}(C-H) -CH_3) and 2935 ν(C-H) aldehydes; 1600 δ(N-H/OH); 1583 ν(C=N); 1488 ν(C=C); 1235 and 836 ν(C=S); 726 ortho-substituted rings; (py). *The IR spectra in detail in the Supplementary materials S13-17.*

3.1.2.(. HL^{2}) N-(3-methoxyphenyl)-2-[(pyridin-2-yl)methylidene]hydrazine-1-carbothioamide

White crystalline solid, yield 96%; mp: 196-197°C, R_f = 0.52 (ethyl acetate-toluene 2:1).. Anal. Calc. for $C_{14}H_{14}N_4OS$: C(58.72%) H(4.93%) N(19.57%). Found: C(58.68%) H(4.82%) N(19.87%). FW: 286.35 g·mol^{-1}. ^{1}H NMR (400 MHz, DMSO-d_6) δ 14.45 (s, 1H, –N*H*-N), 12.09 (s, 1H, –N^4*H*), 10.02 (d, 1H, Py), 8.60 (d, 1H, Py), 8.59 (d, 1H, Py), 7.98(d, 1H, Py), 7.86 (s, 1H, CH=N-), 7.42-6.95 (C-H, Ar), 3.86 (s, 3H, -O–CH_3). ^{13}C NMR (101 MHz, DMSO-d_6) δ 176.6 (C=S); 159.5 (HC=N), 153.4, 149.8, 143.5, 140.5, 137.1, 129.3, 124.8, 121.3, 118.4, 111.9, 111.4 (C-Ar and Py); 55.6 (-O–CH_3). (FTIR (cm^{-1}): 3076 ν (C-H); 2988 ν_{as}(C-H) (sp^3); 2833 ν_{sy}(C-H) (sp^3); 1598 ν(C=N); 1492 ν(C=C); 741 ν(CS).

 doi:10.20944/preprints202411.1900.v1

3.1.3.(. HL^3) N-(4-methoxyphenyl)-2-[(pyridin-2-yl)methylidene]hydrazine-1-carbothioamide

White crystalline solid, yield 97%; mp: 167-168°C, R_f = 0.63 (ethyl acetate-toluene 2:1). Anal. Calc. for $C_{14}H_{14}N_4OS$: C(58.72%) H(4.93%) N(19. Found: C(58.88%) H(4.71%) N(19.66%). FW: 286.35 g·mol^{-1}. ^{1}H NMR (400 MHz, DMSO-d_6) δ 14.36 (s, 1H, –N*H*-N), 11.97 (s, 1H, –N^4*H*), 10.19, 8.59, 8.58, 8.44, 8.42, 8.19, 7.87, 7.84, 7.83 (s, 1H, CH=N-), 7.41-6.94 (C-H, Ar), 3.77 (s, 3H, -O–CH_3). ^{13}C NMR (101 MHz, DMSO-d_6) δ 177.2 (C=S); 157.5 (HC=N), 153.6, 149.8, 143.2, 136.9, 132.2, 128.1, 124.6, 121.1, 113.8(C-Ar and Py); 55.7(-O–CH_3).FTIR (cm^{-1}): 3076 ν (C-H); 2988 ν_{as}(C-H) (sp^3); 2833 ν_{sy}(C-H) (sp^3); 1598 ν(C=N); 1492 ν(C=C); 741 ν(CS).

3.1.4.(. HL^4) N-(3-methoxyphenyl)-2-[1-(pyridin-2-yl)ethylidene]hydrazine-1-carbothioamide

White crystalline solid, yield 92%; mp: 137-138°C, R_f = 0.39 (ethyl acetate-toluene 2:1). Anal. Calc. for $C_{15}H_{16}N_4OS$: C(59.98%) H(5.37%) N(18.65%). Found: C(59.71%) H(5.44%) N(18.81%). FW: 300.37 g·mol^{-1}. ^{1}H NMR (400 MHz, DMSO-d_6) δ 14.60 (s, 1H, –N*H*-N), 11.00 (s, 1H, –N^4*H*), 10.69-6.80 (C-H, Ar and Py), 3.78 (s, 3H, -O–CH_3), 2.48 (s, 3H, -CH_3). ^{13}C NMR (101 MHz, DMSO-d_6) δ 177.47 (C=S), 159.55 (>C=N); 154.96, 149.76, 149.05, 148.9, 140.6, 136.9, 136.9, 129.2, 124.6, 121.7, 121.3, 118.5, 112.0, 111.4 (C-Ar and Py); 55.6 (-O–CH_3); 13.0 (–CH_3). FTIR (cm^{-1}): 3076 ν (C-H); 2988 ν_{as}(C-H) (sp^3); 2833 ν_{sy}(C-H) (sp^3); 1598 ν(C=N); 1492 ν(C=C); 741 ν(CS).

3.1.5. **(HL^5)** *N*-(3-methoxyphenyl)-2-[phenyl(pyridin-2-yl)methylidene]hydrazine-1-carbothioamide

White crystalline solid, yield 90%; mp: 189-190°C, R_f = 0.55 (ethyl acetate-toluene 2:1). Anal. Calc. for $C_{20}H_{18}N_4OS$: C(66.28%) H(5.01%) N(15.46%). Found: C(66.40%) H(4.91%) N(15.95%). FW: 362.44 g·mol^{-1}. ^{1}H NMR (400 MHz, DMSO-d_6) δ 13.16 (s, 1H, –N*H*-N), 10.27 (s, 1H, –N^4*H*), 8.89 (s, 1H, HC=N), 8.07-6.80 (C-H, Ar and Py), 3.76 (s, 3H, -O–CH_3). ^{13}C NMR (101 MHz, DMSO-d_6) δ 176.7(C=S), 159.5 (>C=N); 151.8, 149.3, 144.4, 140.3, 138.7, 137.1, 129.8, 129.6, 128.8, 126.7, 125.5, 118.1, 111.5, 111.5(C-Ar and Py); 55.6 (-O–CH_3). FTIR (cm^{-1}): 3076 ν (C-H); 2988 ν_{as}(C-H) (sp^3); 2833 ν_{sy}(C-H) (sp^3); 1598 ν(C=N); 1492 ν(C=C); 741 ν(CS).

3.2. Synthesis of copper(II) complexes (C1-10)

[Cu(L^1)Cl] (C1)

The equimolar mixture of copper(II) chloride and the ligand (HL^1) in ethyl alcohol was stirred at reflux for 2 hours. The precipitate obtained was filtered and washed with cold ethanol, then recrystallized from ethyl alcohol. The obtained product has a dark green color. Yield: 91%. Anal. Calc. for $C_{14}H_{13}ClCuN_4OS$: C(43.75%) H(3.41%) Cu(16.53%) N(14.58%). Found : C(44.01%) H(3.98%) Cu(16.93%) N(14.77%). FW: 384.34 g·mol^{-1}. FTIR (cm^{-1}): 3401 (N^{4}H/OH); 3076 ν (C-H); 2988 ν_{as}(C-H) (sp^3); 2833 ν_{sy}(C-H) (sp^3); 1598 ν(C=N); 1492 ν(C=C); 741 ν(CS). Molar electrical conductivity (EtOH-DMSO, 9:1): 67 μS/cm. *Supplementary Materials S18–27 display detailed IR spectra for complexes C1–10.*

[Cu(L^1)NO_3] (C2)

The synthesis of compound 2 followed the synthesis protocol for compound 1. The obtained product has a green color. Yield: 83%. Anal. Calc. for $C_{14}H_{13}CuN_5O_4S$: C(40.92%) H(3.19%) Cu(15.47%) N(17.04%). Found: C(41.02%) H(3.40%) Cu(16.07%) N(16.94%). FW: 410.89 g·mol^{-1}. FTIR (cm^{-1}): 3392(N^{4}H/OH); 3040 ν (C-H); 2986 ν_{as}(C-H) (sp^3); 2844 ν_{sy}(C-H) (sp^3); 1597 ν(C=N); 1492 ν(C=C); 750 ν(CS). Molar electrical conductivity (EtOH-DMSO, 9:1): 52 μS/cm.

[Cu(L^2)Cl] (C3)

The synthesis of compound 3 followed the synthesis protocol for compound 1. The obtained product has a green color. Yield: 90%. Anal. Calc. for $C_{14}H_{13}ClCuN_4OS$: C(43.75%) H(3.41%) Cu(16.53%) N(14.58%). Found: C(44.12%) H(3.71%) Cu(16.97%) N(14.59%). FW: 384.34 g·mol^{-1}. FTIR (cm^{-1}): 3356(N^{4}H/OH); 3081 ν (C-H); 2937 ν_{as}(C-H) (sp^3); 2836 ν_{sy}(C-H) (sp^3); 1565 ν(C=N); 1488 ν(C=C); 752 ν(CS). Molar electrical conductivity (EtOH-DMSO, 9:1): 61 μS/cm. Complex **C-3** was recrystallized from DMF, and as a result, the new compound [$Cu_2(L_2)2Cl_2$]·2DMF (C3a) was obtained. Molar electrical conductivity of [$Cu_2(L_2)2Cl_2$]·2DMF (C3a) (DMF): 46 μS/cm.

[Cu(L^2)NO_3] (C4)

 doi:10.20944/preprints202411.1900.v1

The synthesis of compound 4 followed the synthesis protocol for compound 1. The obtained product has a green color. Yield: 75%. Anal. Calc. for $C_{14}H_{13}CuN_5O_4S$: C(40.92%) H(3.19%) Cu(15.47%) N(17.04%). Found: C(41.10%) H(3.34%) Cu(15.97%) N(17.04%). FW: 410.89 g·mol^{-1}. FTIR (cm^{-1}): 3405 (N^4H/OH); 3083 ν (C-H); 2995 ν_{as}(C-H) (sp^3); 2867 ν_{sy}(C-H) (sp^3); 1596 ν(C=N); 1483 ν(C=C); 740 ν(CS). Molar electrical conductivity (EtOH-DMSO, 9:1): 49 μS/cm.

[Cu(L^3)Cl] (C5)

The synthesis of compound 5 followed the synthesis protocol for compound 1. The obtained product has a green color. Yield: 91%. Anal. Calc. for $C_{14}H_{13}ClCuN_4OS$: C(43.75%) H(3.41%) Cu(16.53%) N(14.58%). Found: C(44.20%) H(3.49%) Cu(16.66%) N(14.77%). FW: 384.34 g·mol^{-1}. FTIR (cm^{-1}): 3458 (N^4H/OH); 3043 ν (C-H); 2940 ν_{as}(C-H) (sp^3); 2856 ν_{sy}(C-H) (sp^3); 1580 ν(C=N); 1494 ν(C=C); 743 ν(CS). Molar electrical conductivity (EtOH-DMSO, 9:1): 55 μS/cm.

[Cu(L^3)NO_3] (C6)

The synthesis of compound 6 followed the synthesis protocol for compound 1. The obtained product has a green color. Yield: 86%. Anal. Calc. for $C_{14}H_{13}CuN_5O_4S$: C(40.92%) H(3.19%) Cu(15.47%) N(17.04%). Found: C(41.19%) H(3.41%) Cu(16.18%) N(16.98%). FW: 410.89 g·mol^{-1}. FTIR (cm^{-1}): 3321 (N^4H/OH); 3059 ν (C-H); 2987 ν_{as}(C-H) (sp^3); 2907 ν_{sy}(C-H) (sp^3); 1596 ν(C=N); 1488 ν(C=C); 738 ν(CS). Molar electrical conductivity (EtOH-DMSO, 9:1): 64 μS/cm.

[Cu(L^4)NO_3] (C7)

The synthesis of compound 7 followed the synthesis protocol for compound 1. The obtained product has a green color. Yield: 89%. Anal. Calc. for $C_{15}H_{15}CuN_5O_4S$: C(42.40%) H(3.56%) Cu(14.95%) N(16.48%). Found: C(42.56%) H(3.71%) Cu(15.01%) N(16.71%). FW: 424.92 g·mol^{-1}. FTIR (cm^{-1}): 3322 (N^4H/OH); 3070 ν (C-H); 2988, 2930 ν_{as}(C-H) (sp^3); 2901, 2833 ν_{sy}(C-H) (sp^3); 1546 ν(C=N); 1483 ν(C=C); 739 ν(CS). Molar electrical conductivity (EtOH-DMSO, 9:1): 70 μS/cm.

[Cu(L^4)Cl] (C8)

The synthesis of compound 8 followed the synthesis protocol for compound 1. The obtained product has a green color. Yield: 82%. Anal. Calc. for $C_{15}H_{15}ClCuN_4OS$: C(45.22%) H(3.80%) Cu(15.95%) N(14.06%). Found: C(45.35%) H(3.98%) Cu(16.09%) N(13.96%). FW: 398.36 g·mol^{-1}. FTIR (cm^{-1}): 3322 (N^4H/OH); 3072 ν (C-H); 2987 ν_{as}(C-H) (sp^3); 2901 ν_{sy}(C-H) (sp^3); 1565 ν(C=N); 1498 ν(C=C); 740 ν(CS). Molar electrical conductivity (EtOH-DMSO, 9:1): 58 μS/cm.

[Cu(L^5)Cl] (C9)

The synthesis of compound 9 followed the synthesis protocol for compound 1. The obtained product has a green color. Yield: 96%. Anal. Calc. for $C_{20}H_{17}ClCuN_4OS$: C(52.17%) H(3.72%) Cu(13.80%) N(12.17%). Found: C(52.17%) H(3.72%) Cu(13.80%) N(12.17%). FW: 460.43 g·mol^{-1}. FTIR (cm^{-1}): 3333 (N^4H/OH); 3080 ν (C-H); 2980 ν_{as}(C-H) (sp^3); 2911 ν_{sy}(C-H) (sp^3); 1551 ν(C=N); 1490 ν(C=C); 784 ν(CS). Molar electrical conductivity (EtOH-DMSO, 9:1): 65 μS/cm.

[Cu(L^5)NO_3] (C10)

The synthesis of compound 10 followed the synthesis protocol for compound 1. The obtained product has a green color. Yield: 96%. Anal. Calc. for $C_{20}H_{17}CuN_5O_4S$: C(49.33%) H(3.52%) Cu(13.05%) N(14.38%). Found: C(49.51%) H(3.81%) Cu(12.98%) N(14.94%). FW: 486.99 g·mol^{-1}. FTIR (cm^{-1}): 3305 (N^4H/OH); 3099, 3058 ν (C-H); 2987 ν_{as}(C-H) (sp^3); 2936 ν_{sy}(C-H) (sp^3); 1541 ν(C=N); 1485 ν(C=C); 783 ν(CS). Molar electrical conductivity (EtOH-DMSO, 9:1): 68 μS/cm.

3.3. FT-IR Spectroscopy

FTIR spectra were recorded at room temperature using the BRUKER ALPHA spectrometer, in the wavelength range 4000–400 cm^{-1}, in the scientific research laboratory "Advanced Materials in Biopharmaceutics and Technics" of the State University of Moldova, Republic of Moldova. The spectral results were interpreted using the OPUS version 7.5 program.

3.4. NMR Spectroscopy

Nuclear Magnetic Resonance (NMR) ^1H, ^{13}C, NMR spectra were recorded at room temperature using the BRUKER DRX-400 spectrometer (State University of Moldova, Republic of Moldova).

 doi:10.20944/preprints202411.1900.v1

Chemical shifts are measured in ppm relative to tetramethylsilane (TMS), as solvents were used: DMSO-d_6. The obtained results were processed using the MestReNova v 14.1.2 program.

3.5. Molar Conductivity

Most dissolved substances in water/protic organic solvents dissociate into ions that conduct electricity. Conductometric analysis was performed on the ADWA AD8000 (pH/mV/EC/TDS and Temperature Meter). Calibration of the electrode (AD 76309) was performed with standard solutions of 1430.0 µS/cm and 12,880.0 µS/cm. Samples were solubilized in H_2O/DMF/DMSO/EtOH or mixtures of the listed solvents. The concentration of the investigated samples was $1 \cdot 10^{-3}$M [59,60]

3.6. Melting Point

The substance sample, dry and finely pulverized beforehand by drying the crystals on a watch glass, is introduced into a capillary with a diameter of about 1 mm welded at one end. The height of the substance layer in the capillary should be 4–6 mm. The substance is introduced into the capillary by repeated "knocks" on a hard surface. Recorded the melting point on the Stuart® SMP10 Apparatus, in the range of ambient temperature to 300 °C with a resolution of 1 °C.

3.7. Thin Layer Chromatographic

Thin-layer chromatography, also called partition chromatography, is based on the differences between the partition coefficients of the substances being separated. The analysis was performed using chromatographic plates (Macherey-Nagel, 0.2 mm Silica gel 60 with fluorescent indicator UV254) [61].

3.8. X-ray Crystallography

The crystal structure of **HL²**, **HL³**, **HL⁵** molecules and $[Cu_2(L^2)_2Cl_2]\cdot 2DMF$ **C3a** have been studied by single crystal X-ray analysis. The crystals suitable for the diffraction study of organic molecules were selected directly from the synthesis, while the crystals of **C3a** were obtained by recrystallization of **C3** in DMF solution.

The X-ray diffraction measurements were performed using an X calibur E diffractometer equipped with a charge-coupled device (CCD) area detector and a graphite monochromator using Mo*Kα* radiation (0.71073 Å), at room temperature (293 K). Data collection and reduction and unit cell determination were possessing using the CrysAlis PRO CCD (Oxford Diffraction Ltd., version 1.171.33.66) software. The SHELXS97 and SHELXL2014/2016 program packages [62,63] were used to solve and refine the structures. The structures were solved by direct methods and refined by full-matrix least-squares on F^2 with anisotropic displacement parameters for all non-hydrogen atoms. The C-bound H–atoms were positioned geometrically and treated as riding atoms using SHELXL default parameters with $U_{iso}(H) = 1.2U_{eq}(C)$ and $U_{iso}(H) = 1.5U_{eq}(CH_3)$; the N-bound H-atoms were found from the difference Fourier maps. The X-ray data and refinement details for **HL²**, **HL³**, **HL⁵** and complex **C3a** are summarized in Table 3. The selected bond distances and angles in **HL²**, **HL³**, **HL⁵** and complex **C3a** have common values and are summarized in Table S1. The H-bonding parameters are given in Table S2.The figures were generated using MERCURY [64].

Table 3. Crystal and Structure Refinement Date for **HL²**, **HL³**, **HL⁵** and complex **C3a.**

Compound	**HL²**	**HL³**	**HL⁵**	**C3a**
CCDC	2400994	2400995	2400996	2400997
Empirical formula	$C_{14}H_{14}N_4O_1S_1$	$C_{14}H_{16}N_4O_2S_1$	$C_{20}H_{18}N_4O_1S_1$	$C_{34}H_{40}Cl_2Cu_2N_{10}O_4S_2$
Formula weight	286.35	304.37	362.44	914.86
Crystal system	monoclinic	triclinic	monoclinic	monoclinic

 doi:10.20944/preprints202411.1900.v1

Space group	$P2_1/c$	P-1	$P2_1/n$	$P2_1/c$
Unit cell dimensions				
a (Å)	14.6756(16)	9.5549(18)	9.7269(6)	7.1034(5)
b (Å)	5.3717(5)	12.804(3)	16.9246(8)	23.3341(19)
c (Å)	18.506(2)	14.078(3)	11.1893(6)	12.2189(10)
α (°)	90	109.966(18)	90	90
β (°)	102.331(10)	97.625(15)	96.043(5)	102.395(7)
γ (°)	90	108.195(19)	90	90.895(7)
V (Å^3)	1425.2(3)	1481.6(6)	1831.8(2)	90
Z	4	4	4	2
ρ_{calc} (g cm^{-3})	1.335	1.365	1.314	1.536
μ_{Mo} (mm^{-1})	0.228	0.229	0.193	0.928
F(000)	600	640	760	940
Crystal size (mm)	0.80x0.05x0.03	0.15x0.07x0.05	0.60x0.17x0.08	0.60x0.10x0.03
θ Range (°)	3.228 – 25.05	2.968–24.499	2.932 – 25.044	3.063 – 25.05
Index range	$-17 \le h \le 10$,	$-11 \le h \le 11$,	$-11 \le h \le 11$,	$-8 \le h \le 8$,
	$-6 \le k \le 3$,	$-14 \le k \le 14$,	$-20 \le k \le 19$,	$-16 \le k \le 27$,
	$-16 \le l \le 22$	$-16 \le l \le 142$	$-13 \le l \le 6$	$-14 \le l \le 14$
Reflections collected /	2519 / 2519	8287 / 4909	5970 / 3238	10960 / 3506
unique	(R_{int} = 0.0297)	(R_{int} = 0.0699)	(R_{int} = 0.0236)	(R_{int} = 0.0672)
Reflections with	1351	1800	2230	2636
$I > 2\sigma(I)$				
Number of refined	182	393	236	247
parameters				
Goodness-of-fit (GOF)	0.998	1.000	1.000	1.003
R (for $I > 2\sigma(I)$)	R_1 = 0.0561,	R_1 = 0.0860,	R_1 = 0.0463,	R_1 = 0.0629,
	wR_2 = 0.1001	wR_2 = 0.1240	wR_2 = 0.1081	wR_2 = 0.1668
R (for all reflections)	R_1 = 0.1227,	R_1 = 0.2230,	R_1 = 0.0763,	R_1 = 0.0864,
	wR_2 = 0.1242	wR_2 = 0.1610	wR_2 = 0.1236	wR_2 = 0.1897
$\Delta\rho_{max}/\Delta\rho_{min}$ (e·Å^{-3})	0.206 / -0.181	0.499 / –0.266	0.179 / –0.199	0.922 / –0.515

3.9. Cell proliferation Resazurin assay

The number of viable HeLa, BxPC-3, RD and MDCK cells were measured using resazurin sodium salt (MERCK) as a reagent.

Triplicate cultures of $1 \cdot 10^4$ cells in 100 µL of stated above medium were incubated at 37 °C, 3% CO_2 in 96-well microtiter plates. Tested compounds were dissolved in dimethyl sulfoxide in order to prepare $1 \cdot 10^{-2}$ M solutions. After that these solutions were diluted with corresponding media, added to each well and incubated for 24 hours. Subsequently 20 µL resazurin indicator solution was added to each well and incubated for 4 hours. At last, the absorbance was read at 570 nm and 600 nm.

The percentage inhibition was calculated according to the formula:

$$\boldsymbol{I}\ (\%) = \mathbf{100} - \frac{\boldsymbol{Abs}_{\mathbf{570\ nm}(\boldsymbol{sample})} - \boldsymbol{Abs}_{\mathbf{600\ nm}(\boldsymbol{sample})}}{\boldsymbol{Abs}_{\mathbf{540\ nm}(\boldsymbol{control})} - \boldsymbol{Abs}_{\mathbf{600\ nm}(\boldsymbol{control})}} \times \mathbf{100}$$

 doi:10.20944/preprints202411.1900.v1

where Abs_{570nm} and Abs_{600nm} stand for absorbance at 570 and 600 nm.

3.10. Cell Proliferation MTT Assay

The MTT method is a colorimetric assay for quantifying viable cells, also known as the mitochondrial reduction assay. In this study, it was employed to assess the potential cytotoxic effects of the tested compounds on the LNCaP, MCF-7, HepG-2 and K-562 cancer cell lines. This assay is based on the metabolic reduction of 3-(4,5-dimethylthiazol-2-yl)-2,5-diphenyltetrazolium bromide (MTT), carried out by the enzyme mitochondrial succinate dehydrogenase in metabolically active mitochondria. This enzyme transforms MTT from a yellow hydrophilic soluble compound to a blue hydrophobic insoluble compound (formazan) by cleaving the tetrazolium ring.

Determining the ability of cells to reduce MTT to formazan after exposure to a compound provides information about the toxicity of the compound being evaluated. The tested compounds were dissolved in a physiological saline solution and DMSO (dimethylsulfoxide), ensuring that the DMSO concentration did not exceed 0.1%. The experiment was performed according to the method described by Mosmann [65].

Suspension cells were harvested using centrifugation (MPW 370 centrifuge). Adherent cells were released from their substrate by trypsinization (0.53 mM EDTA, Lonza, Belgium). Cell dilutions (5×10^4 cells per ml) were prepared in culture medium (RPMI 1640 medium, 90% (Merck), containing 10% fetal bovine serum (Invitrogen)). A total of 5×10^3 cells/100 µl of the dilutions were plated into 96-well microtiter plates in triplicate. The cells were incubated for 2-3 hours to allow for attachment.

The tested compounds (10 µl) at three concentrations (0.1 µM, 1 µM, and 10 µM) were added to the wells, with three replicate tests for each concentration, and incubated for 24 hours at 37°C and 3% CO_2 (SANYO CO_2 incubator). Subsequently, 10 µl of MTT reagent (ATCC) was added to each well, including the controls (cells without treatment). The plates were returned to the cell culture incubator for an additional 24 hours, periodically viewing the cells under an inverted microscope (OLYMPUS CK40) for the presence of intracellular punctate purple precipitate. Consequently, this transformation enables the determination of the mitochondrial function of the treated cells, which serves as a measure of cellular viability. It is important to note that mitochondria in dead cells are unable to respire.

When the purple precipitate was clearly visible under the microscope, 100 µl of detergent reagent (ATCC) was added to all wells, including controls. The plates were covered and left in the dark for 4 hours at room temperature. The optical absorbance was measured at 540 nm using a Synergy multi-mode microplate reader (BioTek).

The cell proliferation MTT assay results were reported, as the percent inhibition of compounds. The percent inhibition was calculated according to the following formula:

$$\boldsymbol{I\ (\%) = 100 - \frac{Abs_{540\ nm(sample)}}{Abs_{540\ nm(control)}} \times 100}$$

The half maximal inhibitory concentration (IC_{50}) was used as an indicator of the efficacy of the experimental compounds on the proliferation of cancer cells. IC_{50} is a quantitative measure of the activity of an antagonist in inhibiting a specific biological or biochemical function in vitro in pharmacological studies.

3.11. $ABTS^{\bullet+}$ radical cation scavenging assay

The $ABTS^{\bullet+}$ radical cation scavenging assay is a widely utilized method for evaluating the antioxidant capacity of various compounds. The principle of this assay is based on the ability of antioxidants to quench or neutralize free radicals, in this case, the $ABTS^{\bullet+}$ radical cation. The tested compounds (antioxidants) are introduced into the solution containing the $ABTS^{\bullet+}$ radical cation. The antioxidants donate hydrogen atoms or electrons to the radical, reducing it back to its non-radical form, which leads to a decrease in the absorbance.

 doi:10.20944/preprints202411.1900.v1

The antioxidant activity was evaluated using the $ABTS^{\bullet+}$ method, following the protocol established by Re et al. [66] with some modifications. The $ABTS^{\bullet+}$ assay is a reliable method for measuring the antioxidant capacity of hydrogen-donating antioxidants and chain-breaking antioxidants.

To generate the $ABTS^{\bullet+}$ radical, a reaction was carried out between a 7 mM solution of ABTS (2,2'-azino-bis(3-ethylbenzothiazoline-6-sulphonic acid)) (Merck) and a 2.45 mM solution of potassium persulfate ($K_2S_2O_8$) (Merck), incubating the mixture at 25°C in the dark for 12 to 20 hours. The resulting solution was then diluted with acetate-buffered saline (0.02 M, pH 6.5) to reach an absorbance of approximately 0.70 ± 0.01 units at 734 nm.

Dilutions of the tested compounds in DMSO were prepared at concentrations ranging from 1 to 100 µM. Subsequently, 20 µl of each dilution was added to a 96-well microtiter plate, followed by the addition of 180 µl of the working $ABTS^{\bullet+}$ solution using a dispensing module of a hybrid reader (BioTek). The absorbance at 734 nm was recorded exactly 30 minutes after incubation at 25°C. All measurements were performed in triplicate, with DMSO serving as the negative control. Blank samples were also prepared using the solvent without $ABTS^{\bullet+}$.

The absorbance measurements were conducted using a hybrid reader (Synergy H1, BioTek). The results were averaged from multiple tests. The percentage of inhibition (I%) of $ABTS^{\bullet+}$ production was calculated using the following equation:

$$\boldsymbol{I}\ (\%) = \frac{\boldsymbol{Abs_{734\,nm_0} - Abs_{734\,nm_1}}}{\boldsymbol{Abs_{734\,nm_0}}} \times \mathbf{100}$$

$Abs_{734\,nm0}$ is the absorbance of the control solution; $Abs_{734\,nm1}$ is the absorbance in the presence of sample solutions or standards for positive controls. The $ABTS^{\bullet+}$ radical cation scavenging assay is a reliable and straightforward method for assessing the antioxidant capacity of synthetic and natural compounds. It serves as a valuable tool in research to identify potential health-promoting substances and to understand their mechanisms of action in combating oxidative stress.

3.12. Acute Toxicity Assay against Daphnia magna

Toxicity for some part of the obtained substances was determined using *Daphnia magna* as it was described in [67].

Daphnia magna originated from a culture maintained parthenogenetically at Institute of Zoology (Laboratory of Systematics and Molecular Phylogeny).

The test design was based on ISO 6341:2012. The test-organisms *Daphnia magna Straus* were fed with *Chlorella vulgaris*. These unicellular algae were grown using aseptic technology to exclude contamination of the culture by bacteria, algae or protozoa. *Chlorella vulgaris* were cultivated in Prat's growth medium containing KNO_3 (1 µM), $MgSO_4{\cdot}7H_2O$ (40 µM), $K_2HPO_4{\cdot}3H_2O$ (400 µM), $FeCl_3{\cdot}6H_2O$ (3.6 µM) in H_2O distilled (adjusted the pH to 7.0, autoclaved and stored at 5°C).

D. magna were maintained in aerated aqueous straw infusion growth media supplemented with $CaCl_2$ (11.76 g/L), $NaHCO_3$ (2.59 g/L), KCl (0.23 g/L), $MgSO_47H_2O$ (4.93 g/L). (pH~7.5±0.2; O_2 ≥6.0 mg/L).

Juveniles were selected according to their size and kept in fresh medium for 24 h. *D. magna* were cultured in Costar® 24-well culture clear sterile multiple well plates covered by a lid to prevent the possibility of contamination and evaporation but at the same time to allow gaseous exchange between air and culture medium. Each well contained 10 daphnids in 1000 µL final volume of each dilution of the tested compounds.

The bioassay was then repeated at the concentrations ranging from 0.1 to 100 µM in order to determine LC_{50} for each compound, including doxorubicin (the positive control). Aqueous straw infusion growth media was used to to dilute the stock solutions to the required concentrations. The final test solutions contained up to 0.1% DMSO and had a final volume of 1 mL. A 0.1% solution of DMSO in aerated medium (pH~7.5±0.2; O_2 ≥6.0 mg/L) was used as a negative control. Throughout the experiment, the juvenile daphnids were incubated at 22 ± 2^0C, using a 16 h / 8 h light/dark cycle (500–1000 lx). The mobility (viability) of the test organisms was observed after the 24 h exposure. The experiment was performed in triplicate.

 doi:10.20944/preprints202411.1900.v1

The daphnids were considered immobilized only if they did not swim during the 15 s which follow gentle agitation of the test and control solutions, even if they could still move their antennae. The percentage of viability (V (%)) of *Daphnia magna* was calculated according to the formula:

$$V(\%) = \frac{N_{(sample)}}{N_{(control)}} \times 100$$

N - Number of viability of *Daphnia magna*

3.13. Statistical analysis

The results of the cell proliferation assay were reported as the percent inhibition of the test and control substances. The half maximal inhibitory concentration (IC_{50}) was used as an indicator of the effectiveness of the experimental compounds on the proliferation of cell lines. According to FDA documents, IC_{50} indicates the concentration of a medicinal substance required for 50% inhibition of the tested reaction in vitro. The toxicity of the compounds was evaluated using the median lethal concentration (LC_{50}). The compounds median lethal concentration that kills 50% of the juvenile daphnids (LC_{50}) values were calculated from the dose-response equation determined by the least squares fit method. All data are presented as means ± standard deviation (SD). Statistical analyses were performed using statistical software.

4. Conclusions

In summary, the novel N^4-methoxyphenyl-thiosemicarbazones of pyridine derivatives thiosemicarbazone **HL^{1-5}** were prepared, and their structure was confirmed using various techniques, such as FTIR, NMR. **HL^2, HL^3, HL^5** and **$[Cu_2(L_2)_2Cl_2]\cdot 2DMF$ C3a** have been studied by single crystal X-ray analysis. In DMSO solution, all **HL^{1-5}** ligands are in the majority form in the ionic tautomerism. All coordination compounds **C1-10** are electrolytes 1:1 type, demonstrated by molar conductivities.

The synthesized compounds were tested against a wide spectrum of cancer cell lines, including LNCaP, MCF-7, HepG-2, K-562, HeLa, BxPC-3, and RD, along with MDCK normal cells, to evaluate their antiproliferative activity and selectivity. Most substances showed significant selective anticancer activity, exceeding that of doxorubicin and cisplatin. The complexes exhibited higher anticancer activity compared to the proligands, with the highest selectivity observed in the complexes. All ligands demonstrated high antiproliferative activity against HL-60 cells, with IC_{50} values ranging from 0.01 to 0.06 μM and a selectivity index reaching up to 10000. The coordination of copper with proligands **HL^1** and **HL^3** significantly enhanced antiproliferative activity, reducing the IC_{50} to 0.03 μM.

Additionally, the antioxidant activity of these compounds was evaluated, showing that all tested ligands and most coordination compounds demonstrated superior antioxidant activity compared to Trolox, with some ligands exhibiting activity up to 12.3 times higher. *In vivo* toxicity studies on *Daphnia magna* indicated that the ligands displayed low toxicity, with LC_{50} values ranging from 13 to 90 μM, often lower than doxorubicin, suggesting moderate toxicity. On the other hand, the coordination complexes were more toxic, with LC_{50} values between 0.5 and 13 μM. These findings underscore the potential of these compounds as effective and safer alternatives in cancer therapy.

Supplementary Materials: The following supporting information can be downloaded at the website of this paper posted on Preprints.org. **Figure S1-10**. ^1H, ^{13}C-NMR spectrum of thiosemicarbazone HL^{1-5}. **Figure S13-17.** FT-IR spectrum of HL^{1-5}. **Figure S18-27.** FT-IR spectrum of the coordination compound $[Cu(L^1)Cl]$ (**C1**), $[Cu(L^1)NO_3]$ (**C2**), $[Cu(L^2)Cl]$ (**C3**), $[Cu(L^2)NO_3]$ (**C4**), $[Cu(L^3)Cl]$ (**C5**), $[Cu(L^3)NO_3]$ (**C6**), $[Cu(L^4)NO_3]$ (**C7**), $[Cu(L^4)Cl]$ (**C8**), $[Cu(L^5)Cl]$ (**C9**), $[Cu(L^5)NO_3]$ (**C10**). **Table S1.** Bond Lengths (Å) and Angles (deg) in **HL^2**, **HL^3**, **HL^5** and **C3a**. **Table S2.** Hydrogen Bond Distances (Å) and Angles (deg) for HL^2, HL^3, HL^5 and C3a

Author Contributions: Conceptualization, A.G.; methodology, R.R. and O.G.; validation, R.R., O.G., V.T., and A.G.; formal analysis, O.G., and R.R.; investigation, D.I., E.M.,D.P., O.G.; resources, V.K., D.P., D. I. and A.G.; data curation A.G.; writing—original draft preparation, O.G., V.T.;

writing—review and editing, R.R., O.G., and A.G.; visualization, A.G, R.R., O.G; supervision, O.G., R.R., A.G.; project administration, A.G.; All authors have read and agreed to the published version of the manuscript.

Data Availability Statement: Data is contained within the article or supplementary material.

Acknowledgments: This work was supported by the subprograms 010602, 010701, and 011202 of the institutional project, as well as by the "Young Researchers 2024-2025" project (24.80012.5007.14TC) and the Research and Innovation Project (24.80012.8007.01SE), Republic of Moldova.

Conflicts of Interest: The authors declare no conflict of interest.

References

1. Islam, M.B.; Islam, M.I.; Nath, N.; Emran, T. Bin; Rahman, M.R.; Sharma, R.; Matin, M.M. Recent Advances in Pyridine Scaffold: Focus on Chemistry, Synthesis, and Antibacterial Activities. *Biomed Res. Int.* **2023**, *2023*, doi:10.1155/2023/9967591.
2. Fuior, A.; Cebotari, D.; Haouas, M.; Marrot, J.; Espallargas, G.M.; Guérineau, V.; Touboul, D.; Rusnac, R. V.; Gulea, A.; Floquet, S. Synthesis, Structures, and Solution Studies of a New Class of [Mo 2 O 2 S 2]-Based Thiosemicarbazone Coordination Complexes. *ACS Omega* **2022**, *7*, 16547–16560, doi:10.1021/acsomega.2c00705.
3. Soares, M.A.; Lessa, J.A.; Mendes, I.C.; Da Silva, J.G.; Dos Santos, R.G.; Salum, L.B.; Daghestani, H.; Andricopulo, A.D.; Day, B.W.; Vogt, A.; et al. N 4-Phenyl-Substituted 2-Acetylpyridine Thiosemicarbazones: Cytotoxicity against Human Tumor Cells, Structure-Activity Relationship Studies and Investigation on the Mechanism of Action. *Bioorganic Med. Chem.* **2012**, *20*, 3396–3409, doi:10.1016/j.bmc.2012.04.027.
4. Biot, C.; Pradines, B.; Sergeant, M.H.; Gut, J.; Rosenthal, P.J.; Chibale, K. Design, Synthesis, and Antimalarial Activity of Structural Chimeras of Thiosemicarbazone and Ferroquine Analogues. *Bioorganic Med. Chem. Lett.* **2007**, *17*, 6434–6438, doi:10.1016/j.bmcl.2007.10.003.
5. Klenc, J.; Raux, E.; Barnes, S.; Sullivan, S.; Duszynska, B.; Bojarski, A.J.; Strekowski, L. Synthesis of 4-Substituted 2- (4-Methylpiperazino) Pyrimidines and Quinazoline Analogs as Serotonin 5-HT 2A Receptor Ligands. *J. Heterocycl. Chem.* **2009**, *46*, 1259–1265, doi:10.1002/jhet.
6. Cunha, S.; Silva, T.L. da One-Pot and Catalyst-Free Synthesis of Thiosemicarbazones via Multicomponent Coupling Reactions. *Tetrahedron Lett.* **2009**, *50*, 2090–2093, doi:10.1016/j.tetlet.2009.02.134.
7. Zhang, X.-H.; Bo-Wang; Tao, Y.-Y.; Ma, Q.; Wang, H.-J.; He, Z.-X.; Wu, H.-P.; Li, Y.-H.; Zhao, B.; Ma, L.-Y.; et al. Thiosemicarbazone-Based Lead Optimization to Discover High-Efficiency and Low-Toxicity Anti-Gastric Cancer Agents. *Eur. J. Med. Chem.* **2020**, *199*, 112349, doi:10.1016/j.ejmech.2020.112349.
8. Ilies, D.C.; Pahontu, E.; Shova, S.; Georgescu, R.; Stanica, N.; Olar, R.; Gulea, A.; Rosu, T. Synthesis, Characterization, Crystal Structure and Antimicrobial Activity of Copper(II) Complexes with a Thiosemicarbazone Derived from 3-Formyl-6-Methylchromone. *Polyhedron* **2014**, *81*, 123–131, doi:10.1016/j.poly.2014.05.074.
9. Gulea, A.; Poirier, D.; Roy, J.; Stavila, V.; Bulimestru, I.; Tapcov, V.; Birca, M.; Popovschi, L. In Vitro Antileukemia, Antibacterial and Antifungal Activities of Some 3d Metal Complexes: Chemical Synthesis and Structure - Activity Relationships. *J. Enzyme Inhib. Med. Chem.* **2008**, *23*, 806–818, doi:10.1080/14756360701743002.
10. Pahontu, E.; Julea, F.; Rosu, T.; Purcarea, V.; Chumakov, Y.; Petrenco, P.; Gulea, A. Antibacterial, Antifungal and in Vitro Antileukaemia Activity of Metal Complexes with Thiosemicarbazones. *J. Cell. Mol. Med.* **2015**, *19*, 865–878, doi:10.1111/jcmm.12508.
11. Bacher, F.; Dömötör, O.; Enyedy, É.A.; Filipović, L.; Radulović, S.; Smith, G.S.; Arion, V.B. Complex Formation Reactions of Gallium(III) and Iron(III/II) with L-Proline-Thiosemicarbazone Hybrids: A Comparative Study. *Inorganica Chim. Acta* **2017**, *455*, 505–513, doi:10.1016/j.ica.2016.06.044.
12. Dobrov, A.; Fesenko, A.; Yankov, A.; Stepanenko, I.; Darvasiová, D.; Breza, M.; Rapta, P.; Martins, L.M.D.R.S.; Pombeiro, A.J.L.; Shutalev, A.; et al. Nickel(II), Copper(II) and Palladium(II) Complexes with Bis-Semicarbazide Hexaazamacrocycles: Redox-Noninnocent Behavior and Catalytic Activity in Oxidation and C–C Coupling Reactions. *Inorg. Chem.* **2020**, *59*, 10650–10664, doi:10.1021/acs.inorgchem.0c01119.
13. Kowol, C.R.; Berger, R.; Eichinger, R.; Roller, A.; Jakupec, M.A.; Schmidt, P.P.; Arion, V.B.; Keppler, B.K. Gallium(III) and Iron(III) Complexes of α-N-Heterocyclic Thiosemicarbazones: Synthesis, Characterization, Cytotoxicity, and Interaction with Ribonucleotide Reductase. *J. Med. Chem.* **2007**, *50*, 1254–1265, doi:10.1021/jm0612618.
14. Patel, E.N.; Lin, L.; Park, H.; Sneller, M.M.; Eubanks, L.M.; Tepp, W.H.; Pellet, S.; Janda, K.D. Investigations of Thiosemicarbazides as Botulinum Toxin Active-Site Inhibitors: Enzyme, Cellular, and Rodent Intoxication Studies. **2024**, doi:10.1021/acsinfecdis.4c00750.

15. Köhler, S.C.; Wiese, M. HM30181 Derivatives as Novel Potent and Selective Inhibitors of the Breast Cancer Resistance Protein (BCRP/ABCG2). *J. Med. Chem.* **2015**, *58*, 3910–3921, doi:10.1021/acs.jmedchem.5b00188.
16. Andreu, J.M.; Perez-Ramirez, B.; Gorbunoff, M.J.; Ayala, D.; Timasheff, S.N. Role of the Colchicine Ring A and Its Methoxy Groups in the Binding to Tubulin and Microtubule Inhibition. *Biochemistry* **1998**, *37*, 8356–8368, doi:10.1021/bi9728553.
17. Dong, X.; Sun, Q.; Shi, X.; Yin, Z.; Zeng, B.; Huang, Z.; Li, X. Co-Modification of Engineered Cellulose Surfaces Using Antibacterial Copper-Thiosemicarbazone Complexes and Flame Retardants. *Surfaces and Interfaces* **2024**, *51*, 104688, doi:10.1016/j.surfin.2024.104688.
18. Alam, M.; Abser, M.N.; Kumer, A.; Bhuiyan, M.M.H.; Akter, P.; Hossain, M.E.; Chakma, U. Synthesis, Characterization, Antibacterial Activity of Thiosemicarbazones Derivatives and Their Computational Approaches: Quantum Calculation, Molecular Docking, Molecular Dynamic, ADMET, QSAR. *Heliyon* **2023**, *9*, e16222, doi:10.1016/j.heliyon.2023.e16222.
19. Kumar, S.; Hansda, A.; Chandra, A.; Kumar, A.; Kumar, M.; Sithambaresan, M.; Faizi, M.S.H.; Kumar, V.; John, R.P. Co(II), Ni(II), Cu(II) and Zn(II) Complexes of Acenaphthoquinone 3-(4-Benzylpiperidyl)Thiosemicarbazone: Synthesis, Structural, Electrochemical and Antibacterial Studies. *Polyhedron* **2017**, *134*, 11–21, doi:10.1016/j.poly.2017.05.055.
20. Shoukat, W.; Hussain, M.; Ali, A.; Shafiq, N.; Chughtai, A.H.; Shakoor, B.; Moveed, A.; Shoukat, M.N.; Milošević, M.; Mohany, M. Design, Synthesis, Characterization and Biological Screening of Novel Thiosemicarbazones and Their Derivatives with Potent Antibacterial and Antidiabetic Activities. *J. Mol. Struct.* **2025**, *1320*, doi:10.1016/j.molstruc.2024.139614.
21. Sharma, N.; Dhingra, N.; Singh, H.L. Design, Spectral, Antibacterial and in-Silico Studies of New Thiosemicarbazones and Semicarbazones Derived from Symmetrical Chalcones. *J. Mol. Struct.* **2024**, *1307*, 138000, doi:10.1016/j.molstruc.2024.138000.
22. Terenti, N.; Lazarescu, A.; Shova, S.; Bourosh, P.; Nedelko, N.; Ślawska-Waniewska, A.; Zariciuc, E.; Lozan, V. Synthesis, X-Ray and Antibacterial Activity of New Copper(II) Thiosemicarbazone Complexes Derived from 4-Formyl-3-Hydroxy-2-Naphthoic Acid. *Inorganica Chim. Acta* **2024**, *571*, doi:10.1016/j.ica.2024.122216.
23. Damit, N.S.H.H.; Hamid, M.H.S.A.; Rahman, N.S.R.H.A.; Ilias, S.N.H.H.; Keasberry, N.A. Synthesis, Structural Characterisation and Antibacterial Activities of Lead(II) and Some Transition Metal Complexes Derived from Quinoline-2-Carboxaldehyde 4-Methyl-3-Thiosemicarbazone. *Inorganica Chim. Acta* **2021**, *527*, 120557, doi:10.1016/j.ica.2021.120557.
24. Zhao, Z.; Shi, Z.; Liu, M.; Liu, X. Microwave-Assisted Synthesis and in Vitro Antibacterial Activity of Novel Steroidal Thiosemicarbazone Derivatives. *Bioorganic Med. Chem. Lett.* **2012**, *22*, 7730–7734, doi:10.1016/j.bmcl.2012.09.083.
25. Soraires Santacruz, M.C.; Fabiani, M.; Castro, E.F.; Cavallaro, L. V.; Finkielsztein, L.M. Synthesis, Antiviral Evaluation and Molecular Docking Studies of N4-Aryl Substituted/Unsubstituted Thiosemicarbazones Derived from 1-Indanones as Potent Anti-Bovine Viral Diarrhea Virus Agents. *Bioorganic Med. Chem.* **2017**, *25*, 4055–4063, doi:10.1016/j.bmc.2017.05.056.
26. Xu, Y.S.; Chigan, J.Z.; Li, J.Q.; Ding, H.H.; Sun, L.Y.; Liu, L.; Hu, Z.; Yang, K.W. Hydroxamate and Thiosemicarbazone: Two Highly Promising Scaffolds for the Development of SARS-CoV-2 Antivirals. *Bioorg. Chem.* **2022**, *124*, 105799, doi:10.1016/j.bioorg.2022.105799.
27. Atasever-Arslan, B.; Kaya, B.; Şahin, O.; Ülküseven, B. A Square Planar Cobalt(II)-Thiosemicarbazone Complex. Synthesis, Characterization, Antiviral and Anti-Inflammatory Potential. *J. Mol. Struct.* **2025**, *1321*, doi:10.1016/j.molstruc.2024.140109.
28. Li, A.; Huang, K.; Pan, W.; Wu, Y.; Liang, Y.; Zhang, Z.; Wu, D.; Ma, L.; Gou, Y. Thiosemicarbazone Mixed-Valence Cu(I/II) Complex against Lung Adenocarcinoma Cells through Multiple Pathways Involving Cuproptosis. *J. Med. Chem.* **2024**, *67*, 9091–9103, doi:10.1021/acs.jmedchem.4c00257.
29. Cebotari, D.; Calancea, S.; Garbuz, O.; Balan, G.; Marrot, J.; Shova, S.; Guérineau, V.; Touboul, D.; Tsapkov, V.; Gulea, A.; et al. Synthesis, Structure and Biological Properties of a Series of Dicopper(Bis-Thiosemicarbazone) Complexes. *New J. Chem.* **2024**, *48*, 12043–12053, doi:10.1039/D4NJ00342J.
30. Tiwari, L.; Leach, C.; Williams, A.; Lighter, B.; Heiden, Z.; Roll, M.F.; Moberly, J.G.; Cornell, K.A.; Waynant, K. V. Binding Mechanisms and Therapeutic Activity of Heterocyclic Substituted Arylazothioformamide Ligands and Their Cu(I) Coordination Complexes. *ACS Omega* **2024**, *9*, 37141–37154, doi:10.1021/acsomega.4c04216.
31. Matsa, R.; Makam, P.; Kaushik, M.; Hoti, S.L.; Kannan, T. Thiosemicarbazone Derivatives: Design, Synthesis and in Vitro Antimalarial Activity Studies. *Eur. J. Pharm. Sci.* **2019**, *137*, 104986, doi:10.1016/j.ejps.2019.104986.
32. Savir, S.; Liew, J.W.K.; Vythilingam, I.; Lim, Y.A.L.; Tan, C.H.; Sim, K.S.; Lee, V.S.; Maah, M.J.; Tan, K.W. Nickel(II) Complexes with Polyhydroxybenzaldehyde and O,N,S Tridentate Thiosemicarbazone Ligands: Synthesis, Cytotoxicity, Antimalarial Activity, and Molecular Docking Studies. *J. Mol. Struct.* **2021**, *1242*, 130815, doi:10.1016/j.molstruc.2021.130815.

33. Subhashree, G.R.; Haribabu, J.; Saranya, S.; Yuvaraj, P.; Anantha Krishnan, D.; Karvembu, R.; Gayathri, D. In Vitro Antioxidant, Antiinflammatory and in Silico Molecular Docking Studies of Thiosemicarbazones. *J. Mol. Struct.* **2017**, *1145*, 160–169, doi:10.1016/j.molstruc.2017.05.054.
34. Aly, A.A.; Abdallah, E.M.; Ahmed, S.A.; Rabee, M.M.; Bräse, S. Transition Metal Complexes of Thiosemicarbazides, Thiocarbohydrazides, and Their Corresponding Carbazones with Cu(I), Cu(II), Co(II), Ni(II), Pd(II), and Ag(I)—A Review. *Molecules* **2023**, *28*, 1–39, doi:10.3390/molecules28041808.
35. Piri, Z.; Moradi-Shoeili, Z.; Assoud, A. New Copper(II) Complex with Bioactive 2–Acetylpyridine-4N-p-Chlorophenylthiosemicarbazone Ligand: Synthesis, X-Ray Structure, and Evaluation of Antioxidant and Antibacterial Activity. *Inorg. Chem. Commun.* **2017**, *84*, 122–126, doi:10.1016/j.inoche.2017.08.005.
36. Oliveira, A.A.; Franco, L.L.; Dos Santos, R.G.; Perdigão, G.M.C.; Da Silva, J.G.; Souza-Fagundes, E.M.; Beraldo, H. Neutron Activation of In(III) Complexes with Thiosemicarbazones Leads to the Production of Potential Radiopharmaceuticals for the Treatment of Breast Cancer. *New J. Chem.* **2017**, *41*, 9041–9050, doi:10.1039/c7nj01547j.
37. Kaya, B.; Gholam Azad, M.; Suleymanoglu, M.; Harmer, J.R.; Wijesinghe, T.P.; Richardson, V.; Zhao, X.; Bernhardt, P. V.; Dharmasivam, M.; Richardson, D.R. Isosteric Replacement of Sulfur to Selenium in a Thiosemicarbazone: Promotion of Zn(II) Complex Dissociation and Transmetalation to Augment Anticancer Efficacy. *J. Med. Chem.* **2024**, *67*, 12155–12183, doi:10.1021/acs.jmedchem.4c00884.
38. Porte, V.; Milunovic, M.N.M.; Knof, U.; Leischner, T.; Danzl, T.; Kaiser, D.; Gruene, T.; Zalibera, M.; Jelemenska, I.; Bucinsky, L.; et al. Chemical and Redox Noninnocence of Pentane-2,4-Dione Bis(S-Methylisothiosemicarbazone) in Cobalt Complexes and Their Application in Wacker-Type Oxidation. *JACS Au* **2024**, *4*, 1166–1183, doi:10.1021/jacsau.4c00005.
39. Milunovic, M.N.M.; Ohui, K.; Besleaga, I.; Petrasheuskaya, T. V.; Dömötör, O.; Enyedy, É.A.; Darvasiova, D.; Rapta, P.; Barbieriková, Z.; Vegh, D.; et al. Copper(II) Complexes with Isomeric Morpholine-Substituted 2-Formylpyridine Thiosemicarbazone Hybrids as Potential Anticancer Drugs Inhibiting Both Ribonucleotide Reductase and Tubulin Polymerization: The Morpholine Position Matters. *J. Med. Chem.* **2024**, *67*, 9069–9090, doi:10.1021/acs.jmedchem.4c00259.
40. Lukmantara, A.Y.; Kalinowski, D.S.; Kumar, N.; Richardson, D.R. Structure-Activity Studies of 4-Phenyl-Substituted 2′-Benzoylpyridine Thiosemicarbazones with Potent and Selective Anti-Tumour Activity. *Org. Biomol. Chem.* **2013**, *11*, 6414–6425, doi:10.1039/c3ob41109e.
41. Cebotari, D.; Calancea, S.; Garbuz, O.; Balan, G.; Marrot, J.; Shova, S.; Guérineau, V.; Touboul, D.; Tsapkov, V.; Gulea, A.; et al. Synthesis, Structure and Biological Properties of a Series of Dicopper(Bis-Thiosemicarbazone) Complexes. *New J. Chem.* **2024**, *48*, 12043–12053, doi:10.1039/d4nj00342j.
42. Lighvan, Z.M.; Ramezanpour, A.; Pirani, S.; Akbari, A.; Jahromi, M.D.; Kermagoret, A.; Heydari, A. Synthesis of Tetranuclear Cyclopalladated Complex Using Thiosemicarbazone Derivative Ligand: Spectral, Biological and Molecular Docking Studies. *J. Mol. Struct.* **2025**, *1321*, 139932, doi:10.1016/j.molstruc.2024.139932.
43. Abreu, K.R.; Viana, J.R.; Oliveira Neto, J.G.; Dias, T.G.; Reis, A.S.; Lage, M.R.; da Silva, L.M.; de Sousa, F.F.; dos Santos, A.O. Exploring Thermal Stability, Vibrational Properties, and Biological Assessments of Dichloro(l-Histidine)Copper(II): A Combined Theoretical and Experimental Study. *ACS Omega* **2024**, doi:10.1021/acsomega.4c05029.
44. Beraldo, H.; Nacif, W.F.; West, D.X. Spectral Studies of Semicarbazones Derived from 3- and 4-Formylpyridine and 3- and 4-Acetylpyridine: Crystal and Molecular Structure of 3-Formylpyridine Semicarbazone. *Spectrochim. Acta - Part A Mol. Biomol. Spectrosc.* **2001**, *57*, 1847–1854, doi:10.1016/S1386-1425(01)00413-9.
45. West, D.X.; Iii, J.J.I.; Kozub, N.M.; Bain, G.A.; Liberta, A.E. Douglas X. West*, Jack J. Ingram III, Nicole M. Kozub, Gordon A. Bain and Anthony E. Liberta Department of Chemistry, Illinois State University, Normal, IL 67690, USA. **1996**, *218*, 213–214.
46. Ketcham, K.A.; Swearingen, J.K.; Castieiras, A.; Garcia, I.; Bermejo, E.; West, D.X. Iron(III), Cobalt(II,III), Copper(II) and Zinc(II) Complexes of 2-Pyridineformamide 3-Piperidylthiosemicarbazone. *Polyhedron* **2001**, *20*, 3265–3273, doi:10.1016/S0277-5387(01)00941-X.
47. Muğlu, H. Synthesis, Spectroscopic Characterization, DFT Studies and Antioxidant Activity of New 5-Substituted Isatin/Thiosemicarbazones. *J. Mol. Struct.* **2025**, *1322*, 140406, doi:10.1016/j.molstruc.2024.140406.
48. Arion, V.B. Coordination Chemistry of S-Substituted Isothiosemicarbazides and Isothiosemicarbazones. *Coord. Chem. Rev.* **2019**, *387*, 348–397, doi:10.1016/j.ccr.2019.02.013.
49. Farzaliyeva, A.; Şenol, H.; Taslimi, P.; Çakır, F.; Farzaliyev, V.; Sadeghian, N.; Mamedov, I.; Sujayev, A.; Maharramov, A.; Alwasel, S.; et al. Synthesis and Biological Studies of Acetophenone-Based Novel Chalcone, Semicarbazone, Thiosemicarbazone and Indolone Derivatives: Structure-Activity Relationship, Molecular Docking, Molecular Dynamics, and Kinetic Studies. *J. Mol. Struct.* **2025**, *1321*, 140197, doi:10.1016/j.molstruc.2024.140197.

50. Chatterjee, K.; Zhang, J.; Honbo, N.; Karliner, J.S. Doxorubicin Cardiomyopathy. *Cardiology* **2010**, *115*, 155–162, doi:10.1159/000265166.
51. Reszka, K.J.; Britigan, B.E. Doxorubicin Inhibits Oxidation of 2,2′-Azino-Bis(3-Ethylbenzothiazoline-6-Sulfonate) (ABTS) by a Lactoperoxidase/H2O2 System by Reacting with ABTS-Derived Radical. *Arch. Biochem. Biophys.* **2007**, *466*, 164–171, doi:10.1016/j.abb.2007.06.027.
52. Kruidering, M.; Van De Water, B.; De Heer, E.; Mulder, G.J.; Nagelkerke, J.F. Cisplatin-Induced Nephrotoxicity in Porcine Proximal Tubular Cells: Mitochondrial Dysfunction by Inhibition of Complexes I to IV of the Respiratory Chain. *J. Pharmacol. Exp. Ther.* **1997**, *280*.
53. Zhang, J.G.; Lindup, W.E. Cisplatin Nephrotoxicity: Decreases in Mitochondrial Protein Sulphydryl Concentration and Calcium Uptake by Mitochondria from Rat Renal Cortical Slices. *Biochem. Pharmacol.* **1994**, *47*, 1127–1135, doi:10.1016/0006-2952(94)90383-2.
54. Kaiafa, G.D.; Saouli, Z.; Diamantidis, M.D.; Kontoninas, Z.; Voulgaridou, V.; Raptaki, M.; Arampatzi, S.; Chatzidimitriou, M.; Perifanis, V. Copper Levels in Patients with Hematological Malignancies. *Eur. J. Intern. Med.* **2012**, *23*, 738–741, doi:10.1016/j.ejim.2012.07.009.
55. Pan, Q.; Kleer, C.G.; Van Golen, K.L.; Irani, J.; Bottema, K.M.; Bias, C.; De Carvalho, M.; Mesri, E.A.; Robins, D.M.; Dick, R.D.; et al. Copper Deficiency Induced by Tetrathiomolybdate Suppresses Tumor Growth and Angiogenesis. *Cancer Res.* **2002**, *62*, 4854–4859.
56. Garbuz, O.; Graur, V.; Graur, I.; Railean, N.; Toderas, I.; Pahontu, E.; Ceban, I.; Jinga, V.; Istrati, D.; Ceban, E.; et al. Biological Activity of Copper(II) Complex (2-((2-(Prop-2-En-1-Ylcarbamothioyl)Hydrazinylidene)Methyl)Phenolato)-Chloro-Copper(II) Monohydrate. *J. Cancer Sci. Clin. Ther.* **2024**, *8*, 287–294, doi:10.26502/jcsct.5079251.
57. Garbuz O., Gudumac V., Toderas I., Gulea A. *Antioxidant properties of synthetic compounds and natural products. Action mechanisms. Monograph.* Chisinau, 2023; ISBN 978-9975-62-516-6.
58. Fujikawa, F.; Hirai, K.; Naito, M.; Tsukuma, S. Studies on Chemotherapeutics for Micobacterium Tuberculosis. Synthesis and Antibacterial Activity on Micobucterium Tuberculosis of Pyridinealdehyde Thiosemicarbazones. *YAKUGAKU ZASSHI* **1959**, *79*, 1231–1234, doi:10.1248/yakushi1947.79.10_1231.
59. Gaber, A.; Refat, M.S.; Belal, A.A.M.; El-deen, I.M.; Hassan, N.; Zakaria, R.; Alhomrani, M.; Alamri, A.S.; Alsanie, W.F.; Saied, E.M. Biological Activity : Antimicrobial and Molecular Docking Study. **2021**, *26*, 1–18.
60. Joseph, M.; Sreekanth, A.; Suni, V.; Kurup, M.R.P. Spectral Characterization of Iron(III) Complexes of 2-Benzoylpyridine N(4)-Substituted Thiosemicarbazones. *Spectrochim. Acta - Part A Mol. Biomol. Spectrosc.* **2006**, *64*, 637–641, doi:10.1016/j.saa.2005.07.067.
61. Touchstone, J.C. Thin-Layer Chromatographic Procedures for Lipid Separation. *J. Chromatogr. B Biomed. Sci. Appl.* **1995**, *671*, 169–195, doi:10.1016/0378-4347(95)00232-8.
62. Sheldrick, G.M. A Short History of SHELX . *Acta Crystallogr. Sect. A Found. Crystallogr.* **2008**, *64*, 112–122, doi:10.1107/s0108767307043930.
63. Sheldrick, G.M. Crystal Structure Refinement with SHELXL. *urn:issn:2053-2296* **2015**, *71*, 3–8, doi:10.1107/S2053229614024218.
64. Macrae, C.F.; Bruno, I.J.; Chisholm, J.A.; Edgington, P.R.; McCabe, P.; Pidcock, E.; Rodriguez-Monge, L.; Taylor, R.; van de Streek, J.; Wood, P.A. Mercury CSD 2.0 – New Features for the Visualization and Investigation of Crystal Structures. *J. Appl. Crystallogr.* **2008**, *41*, 466–470, doi:10.1107/S0021889807067908.
65. Mosmann, T. Rapid Colorimetric Assay for Cellular Growth and Survival: Application to Proliferation and Cytotoxicity Assays. *J. oflmmunological Methods* **1983**, *65*, 55–63.
66. Re, R.; Pellegrini, N.; Proteggente, A.; Pannala, A.; Yang, M.; Rice-Evans, C. Antioxidant Activity Applying an Improved ABTS Radical Cation Decolorization Assay. *Free Radic. Biol. Med.* **1999**, *26*, 1231–1237, doi:10.1016/S0891-5849(98)00315-3.
67. Graur, V.; Chumakov, Y.; Garbuz, O.; Hureau, C.; Tsapkov, V.; Gulea, A. Synthesis, Structure, and Biologic Activity of Some Copper, Nickel, Cobalt, and Zinc Complexes with 2-Formylpyridine N 4 - Allylthiosemicarbazone. *Bioinorg. Chem. Appl.* **2022**, *2022*, doi:10.1155/2022/2705332.